Extraction of Double Spin Asymmetries from pp2pp 2009 run data. Analysis note.

I. Alekseev, L. Koroleva, B. Morozov, D. Svirida

ITEP, Moscow

September 23, 2013

Abstract

The note describes details of the analysis aimed at the extraction of double spin asymmetries from the data of pp2pp dedicated run in 2009 with the highest achievable accuracy. The analysis uses BBC coincidence counts for relative luminosity calculations. The results show small negative values for $(A_{NN} + A_{SS})/2$ and are compatible with zero for $(A_{NN} - A_{SS})/2$.

Contents

1 Introduction

Transverse double spin asymmetries A_{NN} and A_{SS} for the elastic proton-proton scattering are expressed in terms of helicity amplitudes, as in [1]:

$$A_{NN}\frac{d\sigma}{dt} = \frac{4\pi}{s^2}\{2|\phi_5|^2 + Re(\phi_1^*\phi_2 - \phi_3^*\phi_4)\} \quad (1)$$

$$A_{SS}\frac{d\sigma}{dt} = \frac{4\pi}{s^2}\{Re(\phi_1\phi_2^* + \phi_3\phi_4^*)\}. \quad (2)$$

In each amplitude, both electromagnetic and nuclear terms should be taken into account in the CNI region. The largest contributions come from ϕ_1 and ϕ_3, the dominant non-spin-flip amplitudes. The hadronic part of ϕ_5 was recently measured to be small in [2], while its electromagnetic part is

kinematically suppressed compared to ϕ_1 and ϕ_3 (see [1]). Thus, neglecting ϕ_5, approximate relations can be derived:

$$\frac{A_{NN}+A_{SS}}{2}\frac{d\sigma}{dt} \approx \frac{4\pi}{s^2}\mathrm{Re}\,\phi_1\phi_2^*\,, \qquad \frac{A_{NN}-A_{SS}}{2}\frac{d\sigma}{dt} \approx -\frac{4\pi}{s^2}\mathrm{Re}\,\phi_3\phi_4^*. \tag{3}$$

Consequently, $A_{NN}+A_{SS}$ is a good probe for ϕ_2, while $A_{NN}-A_{SS}$ is generally sensitive to ϕ_4, but expected to be close to zero because the latter amplitude is kinematically suppressed.

Due to the above considerations, the following analysis will refer to the combinations $(A_{NN}+A_{SS})/2$ and $(A_{NN}-A_{SS})/2$ as bearing distinct physics information, rather than to the double spin asymmetries A_{NN} and A_{SS} themselves.

To quantify the spin-dependent hadronic contributions, the relative amplitudes are usually introduced, see, for example, [3]:

$$r_2 = \frac{\phi_2^{had}}{2\ \mathrm{Im}\,\phi_+^{had}} \qquad r_5 = \frac{m_p\phi_5^{had}}{\sqrt{-t}\ \mathrm{Im}\,\phi_+^{had}} \qquad r_4 = -\frac{m_p^2\phi_4^{had}}{t\ \mathrm{Im}\,\phi_+^{had}}. \tag{4}$$

These amplitudes already include main kinematic factors and their $(-t)$ dependence in small regions is usually neglected. The amplitudes are related to the value of the dominant non-spin-flipping amplitude $\phi_+^{had} = (\phi_1^{had}+\phi_3^{had})/2$.

Using relative amplitudes the approximate explicit expressions for the double spin asymmetries can be written to describe their $(-t)$ dependence, see appendix A:

$$\frac{A_{NN}+A_{SS}}{2} = 2\cdot\frac{(\rho-\frac{t_c}{t})\mathrm{Re}\,r_2+(1-\delta\frac{t_c}{t})\mathrm{Im}\,r_2}{\left(\frac{t_c}{t}\right)^2-2(\rho+\delta)\frac{t_c}{t}+1+\rho^2}\,, \tag{5}$$

$$\frac{A_{NN}-A_{SS}}{2} = \frac{t}{m^2}\cdot\frac{(\rho-\frac{t_c}{t})\mathrm{Re}\,r_4+(1-\delta\frac{t_c}{t})\mathrm{Im}\,r_4}{\left(\frac{t_c}{t}\right)^2-2(\rho+\delta)\frac{t_c}{t}+1+\rho^2}\,. \tag{6}$$

The above formulas and their applicability in the $(-t)$ range of this work were discussed with [4, 5] in private communication. Nevertheless the full set of exact formulas (A.13–A.27) was used for the extraction of the relative amplitudes.

2 Analysis basics

The set of the elastic events selected for this analysis is exactly the same as the one used for the single spin asymmetry calculations by [2]. The details of the detector alignment, hit treatment and elastic event selection can be found in [6]. The division of the data into bins in momentum transferred is also exactly the same as in [2, 6].

For the transversely polarized beams the angular distribution of the elastically scattered protons is given by the general formula:

$$2\pi\frac{d^2\sigma}{dtd\varphi} = \frac{d\sigma}{dt}\left(1+(P_B+P_Y)A_N\cos\varphi+P_BP_Y(A_{NN}\cos^2\varphi+A_{SS}\sin^2\varphi)\right), \tag{7}$$

where P_B and P_Y are the signed values of the polarization of the two beams. The double spin term can be expressed in the form:

$$\varepsilon_2(\varphi) = P_BP_Y((A_{NN}+A_{SS})/2+(A_{NN}-A_{SS})/2\cdot\cos 2\varphi). \tag{8}$$

Thus, while $(A_{NN}-A_{SS})/2$ can be extracted from the angular distributions, $(A_{NN}+A_{SS})/2$ effectively manifests only as the cross-section difference for parallel and anti-parallel combinations of the beam spin directions.

In this case the 'square root formula' [7] cannot be applied and one is bound to rely on normalized event counts, K^{by}, for the extraction of the raw double spin asymmetries:

$$\varepsilon_2(\varphi) = \varepsilon_2' + \varepsilon_2'' \cos 2\varphi = \frac{(K^{++}(\varphi) + K^{--}(\varphi)) - (K^{+-}(\varphi) + K^{-+}(\varphi))}{(K^{++}(\varphi) + K^{--}(\varphi)) + (K^{+-}(\varphi) + K^{-+}(\varphi))}. \tag{9}$$

In this formula $K^{by}(\varphi) = N^{by}(\varphi)/L^{by}$, $N^{by}(\varphi)$ are the elastic event counts in a certain small bin of azimuthal angle φ for certain spin combinations in 'blue' and 'yellow' beams $b, y = +$ or $-$, and L^{by} are the counts of the luminosity monitor for these combinations. It's worth mentioning that in this approach the acceptance asymmetries of the setup are fully cancelled out, but the normalization counts L^{by} play the main role in the uncertainty of the result.

The choice of the luminosity monitor is crucial for this analysis. Several STAR and RHIC subsystems were thoroughly investigated in [8] to select the most appropriate source of normalization. BBC coincidence count was proved to be least of all sensitive to the double spin effects, while its statistical error can be neglected because of huge amount of data. This count with additional restrictions on the coincidence properties and corrected for accidentals and multiplicity is used for normalized count calculations.

For the main flow of the analysis the angular bins of 5^o are chosen. The data is analyzed on the run by run basis and the raw asymmetries $\varepsilon_2(\varphi)/(P_B P_Y)$ are obtained for each run and each of the $(-t)$ bins as the first step. The values of the beam polarizations [9] and their products are summarized in the table 1. The total errors on the polarization products are calculated using the equation:

$$\frac{\delta(P_B \cdot P_Y)}{P_B \cdot P_Y} = \sqrt{\left(\frac{\delta P_B}{P_B}\right)^2 + \left(\frac{\delta P_Y}{P_Y}\right)^2 + \delta_{GLOB}^2}\,, \tag{10}$$

where δ_{GLOB} is 6.5% global run 2009 $\sqrt{s} = 200$ GeV polarization product systematic error [9].

On the next step the results of individual runs are averaged error-weighted to obtain final $\varepsilon_2(\varphi)/(P_B P_Y)$ distributions for each $(-t)$ bin. Only statistical errors are taken into account in the weighting process. The basic fit with a constant plus $\cos 2\varphi$ function is applied then to each distribution in accordance with (8) and double spin combinations $(A_{NN} + A_{SS})/2$ and $(A_{NN} - A_{SS})/2$ are obtained with the statistical error given by the fit. Figure 1 illustrates the fitting procedure for the main flow of the analysis with the elastic event selection cut $\chi^2 < 9$ and fiducial volume cuts applied as in [2, 6]. The upper left panel corresponds to the average over the whole $(-t)$-range of the experiment, while other 5 sub-figures represent results for individual $(-t)$-bins. The values of the $(-t)$-range boundaries and statistically weighted central values can be found in the head lines of the table 2. The obtained fit results are given in bold in the same table. Numeric values of $(A_{NN} - A_{SS})/2$ are nearly compatible with zero, while the numbers for $(A_{NN} + A_{SS})/2$ are negative and deviate from zero at the level of 4-5 standard errors. The reasonable quality of the fits is justified by the moderate values of χ^2.

3 Stability tests

In addition to the main analysis flow several deviations from it were undertaken to check the stability of the results. The summary of various test results is presented in tab. 2 together with the main fit values. Each line in the table refers to the corresponding figure, illustrating the quality of the fit.

The first test is intended to check for the residual single spin effect in the raw asymmetry angular dependence and for this purpose $\cos\varphi$ term was added to the fit function. From fig. 2 one can see, that addition of the third parameter does not lead to any χ^2 reduction, while the values of the single spin term are compatible with zero in most cases. It is also natural that the changes of the constant

and $\cos 2\varphi$ terms are small compared to their statistical errors due to the orthogonality of the Fourier decomposition on the angular interval $(-\pi;\pi)$ of the experiment.

The second fit (fig. 3) is made with a constant term only and results in small increase of the fit χ^2. The values obtained for $(A_{NN}+A_{SS})/2$ in this case do not significantly deviate from the original ones. These two observations are also quite natural because of the mentioned Fourier decomposition property and because of the fact that the $\cos 2\varphi$ term is close to zero in the original distribution.

The third test (fig. 4) justifies the independence of the results on the number of angular intervals. Asymmetry data is rebinned into 10^o intervals which is twice the size of the original bins. No change of the resulting values is observed at the level of $1\cdot 10^{-4}$. Also the fits χ^2 values related to the number of degrees of freedom remain unchanged.

The next fit (fig. 5) is made to the data obtained with removed fiducial volume cut. The numbers show extreme stability.

The two following tests are devoted to the quality of the elastic event selection by means of reconstruction χ^2 criteria. In the main flow of this analysis the cut condition is chosen as $\chi^2 < 9$ according to [2, 6]. Figure 6 represents stronger cut $\chi^2 < 4$. Most numbers deviate from the main flow not greater than by half of the statistical error except for the first two $(-t)$-bins where the deviation is about one standard. Fit χ^2 values are slightly reduced. Figure 7 is for the weaker $\chi^2 < 20$ cut. Though the deviation absolute values are similar to the previous test, the direction of the change is opposite in most cases. Such behaviour of the results suggests further studies of the systematic errors accociated with the subjective choice of the reconstruction χ^2 cut.

The last three tests are actually the numerical calculations of partial derivatives of the asymmetries on the independent normalization ratios R_j, see [8] for details. Each of the ratios R_2, R_B and R_Y, one by one, were given an increment of 0.0005, corresponding r_{by} ratios were recalculated for each run, and the full analysis was repeated to obtain the fit results for the perturbed data.

As expected, disturbance of $(A_{NN}-A_{SS})/2$ values is totally zero. With double spin ratio R_2 perturbation, $(A_{NN}+A_{SS})/2$ is anticipated to receive a shift of

$$\Delta\left(\frac{A_{NN}+A_{SS}}{2}\right) = -\frac{2}{P_B P_Y}\Delta R_2 \approx -\frac{2}{0.37}5\cdot 10^{-4} = -2.7\cdot 10^{-3}. \qquad (11)$$

and this is exactly what is observed in the table 2 (third row from the bottom). For this estimate we took approximate average of polarization product as arithmetic mean of the four fills $<P_B P_Y> \approx 0.37$.

The derivatives on the single spin ratios R_B and R_Y are expected to be of the order of 10^{-2} and dependent on the particular missing bunch pattern. The last two rows of the table proof the algebraic conclusions: no changes are seen for $(A_{NN}+A_{SS})/2$ values at the level of $1\cdot 10^{-4}$. Since the perturbation values $\Delta R_{B,Y} = 5\cdot 10^{-4}$ are close to the experimental uncertainty on these ratios, the statement that these uncertainties can be safely neglected is thus fully justified.

The performed tests demonstrate reasonable stability of the results to the variations of the main analysis algorithm and justified the theoretical approach to the systematics introduced by the uncertainties in the normalization ratios. At the same time they suggest further studies of the systematic errors due to the choice of the elastic event selection χ^2 cut.

Table 1: Beam polarizations during the dedicated large β^* fills in 2009.

Fill No	P_B	P_Y	$P_B \cdot P_Y$	Runs
11020	0.623 ± 0.052	0.621 ± 0.071	0.387 ± 0.060	10181085, 10181086, 10182001, 10182002, 10182004, 10182005, 10182006, 10182015, 10182016, 10182021, 10182025
11026	0.548 ± 0.051	0.590 ± 0.048	0.323 ± 0.045	10183013, 10183014, 10183015, 10183016, 10183017, 10183018, 10183020, 10183021, 10183027, 10183028, 10183034, 10183035, 10183037, 10183038
11030	0.620 ± 0.053	0.644 ± 0.051	0.399 ± 0.053	10184016, 10184017, 10184018, 10184019, 10184020, 10184021, 10184030, 10184031, 10184032, 10184033
11032	0.619 ± 0.054	0.618 ± 0.048	0.383 ± 0.051	10185001, 10185002, 10185003, 10185004, 10185005, 10185006, 10185016, 10185018, 10185019, 10185020, 10185023

Table 2: Results of the fits.

Parameter	$(-t)$-range, $(\mathrm{GeV/c})^2$						Comment
	all	0.003-0.005	0.005-0.010	0.010-0.015	0.015-0.020	0.020-0.035	
$< -t >$, $(\mathrm{GeV/c})^2$		0.0039	0.0077	0.0126	0.0175	0.0232	
$(A_{NN} + A_{SS})/2$	$\mathbf{-0.0060 \pm 0.0006}$	$\mathbf{-0.0140 \pm 0.0039}$	$\mathbf{-0.0063 \pm 0.0014}$	$\mathbf{-0.0060 \pm 0.0011}$	$\mathbf{-0.0064 \pm 0.0011}$	$\mathbf{-0.0035 \pm 0.0014}$	**The main fit ($\chi^2 < 9$).**
$(A_{NN} - A_{SS})/2$	$\mathbf{0.0015 \pm 0.0009}$	$\mathbf{0.0112 \pm 0.0052}$	$\mathbf{0.0023 \pm 0.0019}$	$\mathbf{0.0024 \pm 0.0016}$	$\mathbf{0.0011 \pm 0.0017}$	$\mathbf{-0.0046 \pm 0.0025}$	**Fig. 1**
$(A_{NN} + A_{SS})/2$	-0.0060 ± 0.0006	-0.0132 ± 0.0040	-0.0060 ± 0.0014	-0.0060 ± 0.0011	-0.0064 ± 0.0011	-0.0037 ± 0.0014	Fit with cosine function
$(A_{NN} - A_{SS})/2$	0.0015 ± 0.0009	0.0118 ± 0.0052	0.0026 ± 0.0019	0.0024 ± 0.0016	0.0010 ± 0.0017	-0.0044 ± 0.0025	included. Fig. 2
A_{RN}	-0.0001 ± 0.0008	-0.0045 ± 0.0038	-0.0026 ± 0.0018	-0.0012 ± 0.0016	-0.0003 ± 0.0016	0.0033 ± 0.0015	
$(A_{NN} + A_{SS})/2$	-0.0058 ± 0.0006	-0.0087 ± 0.0031	-0.0059 ± 0.0013	-0.0059 ± 0.0011	-0.0064 ± 0.0011	-0.0048 ± 0.0012	Fit with constant term only. Fig. 3
$(A_{NN} + A_{SS})/2$	-0.0060 ± 0.0006	-0.0140 ± 0.0039	-0.0062 ± 0.0014	-0.0060 ± 0.0010	-0.0064 ± 0.0011	-0.0036 ± 0.0014	Fit with twice larger
$(A_{NN} - A_{SS})/2$	0.0014 ± 0.0009	0.0112 ± 0.0052	0.0019 ± 0.0019	0.0024 ± 0.0016	0.0011 ± 0.0017	-0.0044 ± 0.0025	angular intervals. Fig. 4
$(A_{NN} + A_{SS})/2$	-0.0060 ± 0.0006	-0.0140 ± 0.0039	-0.0063 ± 0.0014	-0.0060 ± 0.0011	-0.0064 ± 0.0011	-0.0037 ± 0.0014	Fit without fiducial volume
$(A_{NN} - A_{SS})/2$	0.0014 ± 0.0009	0.0112 ± 0.0052	0.0023 ± 0.0019	0.0024 ± 0.0016	0.0009 ± 0.0016	-0.0044 ± 0.0024	cut. Fig. 5
$(A_{NN} + A_{SS})/2$	-0.0061 ± 0.0006	-0.0099 ± 0.0042	-0.0056 ± 0.0015	-0.0065 ± 0.0012	-0.0066 ± 0.0012	-0.0038 ± 0.0015	Strong χ^2 cut: $\chi^2 < 4$
$(A_{NN} - A_{SS})/2$	0.0010 ± 0.0009	0.0049 ± 0.0055	0.0011 ± 0.0020	0.0021 ± 0.0017	0.0015 ± 0.0018	-0.0055 ± 0.0027	Fig. 6
$(A_{NN} + A_{SS})/2$	-0.0068 ± 0.0006	-0.0201 ± 0.0038	-0.0083 ± 0.0014	-0.0065 ± 0.0011	-0.0067 ± 0.0011	-0.0039 ± 0.0014	Weak χ^2 cut: $\chi^2 < 20$
$(A_{NN} - A_{SS})/2$	0.0025 ± 0.0009	0.0177 ± 0.0050	0.0052 ± 0.0019	0.0024 ± 0.0016	0.0013 ± 0.0016	-0.0041 ± 0.0025	Fig. 7
$(A_{NN} + A_{SS})/2$	-0.0087 ± 0.0006	-0.0166 ± 0.0039	-0.0090 ± 0.0014	-0.0087 ± 0.0011	-0.0091 ± 0.0011	-0.0062 ± 0.0014	$\Delta R_2 = 0.0005$ Fig. 8
$(A_{NN} - A_{SS})/2$	0.0015 ± 0.0009	0.0112 ± 0.0052	0.0023 ± 0.0019	0.0024 ± 0.0016	0.0011 ± 0.0017	-0.0046 ± 0.0025	
$(A_{NN} + A_{SS})/2$	-0.0060 ± 0.0006	-0.0140 ± 0.0039	-0.0063 ± 0.0014	-0.0060 ± 0.0011	-0.0065 ± 0.0011	-0.0036 ± 0.0014	$\Delta R_B = 0.0005$ Fig. 9
$(A_{NN} - A_{SS})/2$	0.0015 ± 0.0009	0.0112 ± 0.0052	0.0023 ± 0.0019	0.0024 ± 0.0016	0.0011 ± 0.0017	-0.0046 ± 0.0025	
$(A_{NN} + A_{SS})/2$	-0.0060 ± 0.0006	-0.0140 ± 0.0039	-0.0063 ± 0.0014	-0.0060 ± 0.0011	-0.0065 ± 0.0011	-0.0036 ± 0.0014	$\Delta R_Y = 0.0005$ Fig. 10
$(A_{NN} - A_{SS})/2$	0.0015 ± 0.0009	0.0112 ± 0.0052	0.0023 ± 0.0019	0.0024 ± 0.0016	0.0011 ± 0.0017	-0.0046 ± 0.0025	

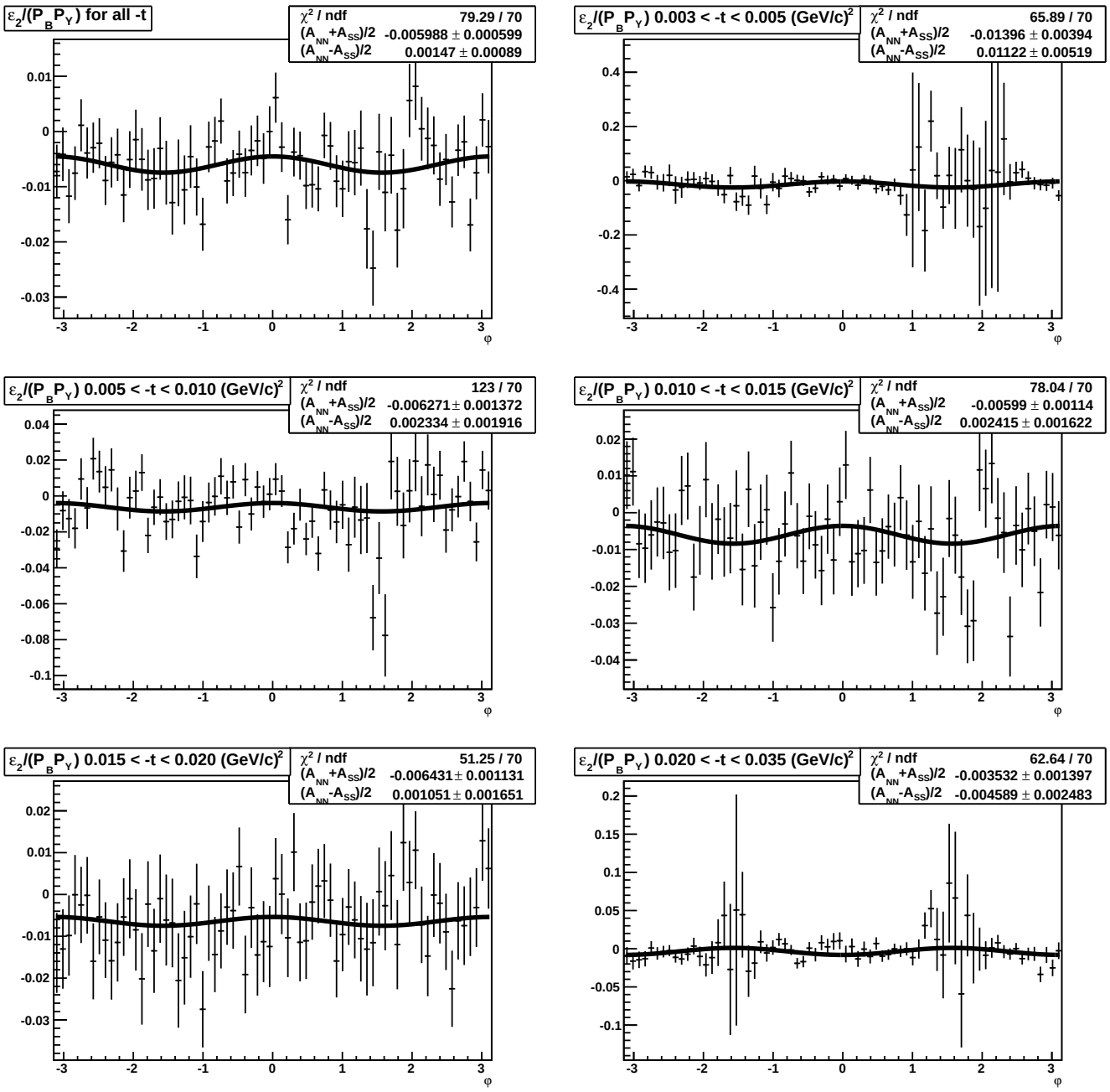

Figure 1: The main fit ($\chi^2 < 9$).

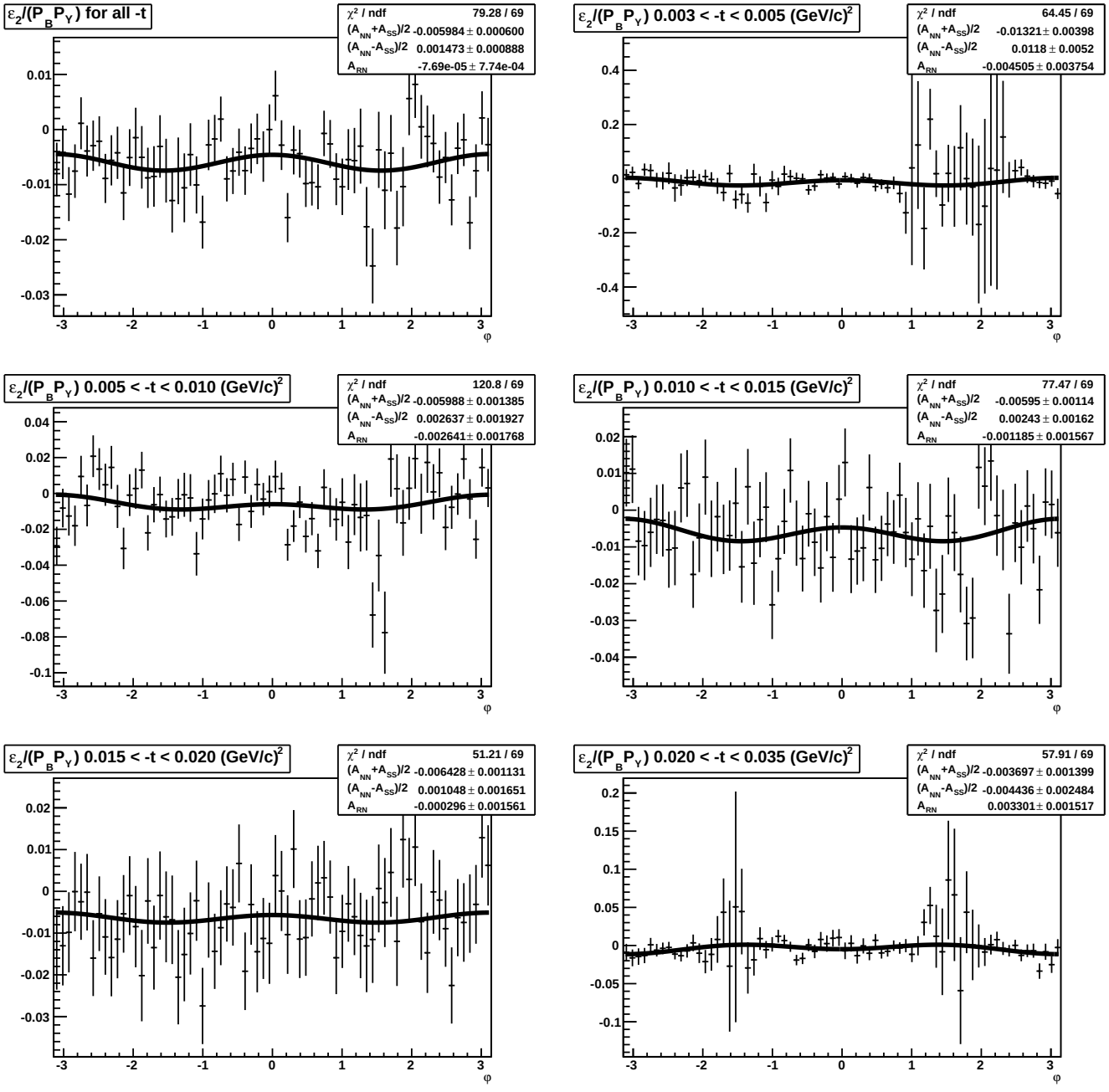

Figure 2: Fit with cosine function added to check for single spin asymmetry residuals.

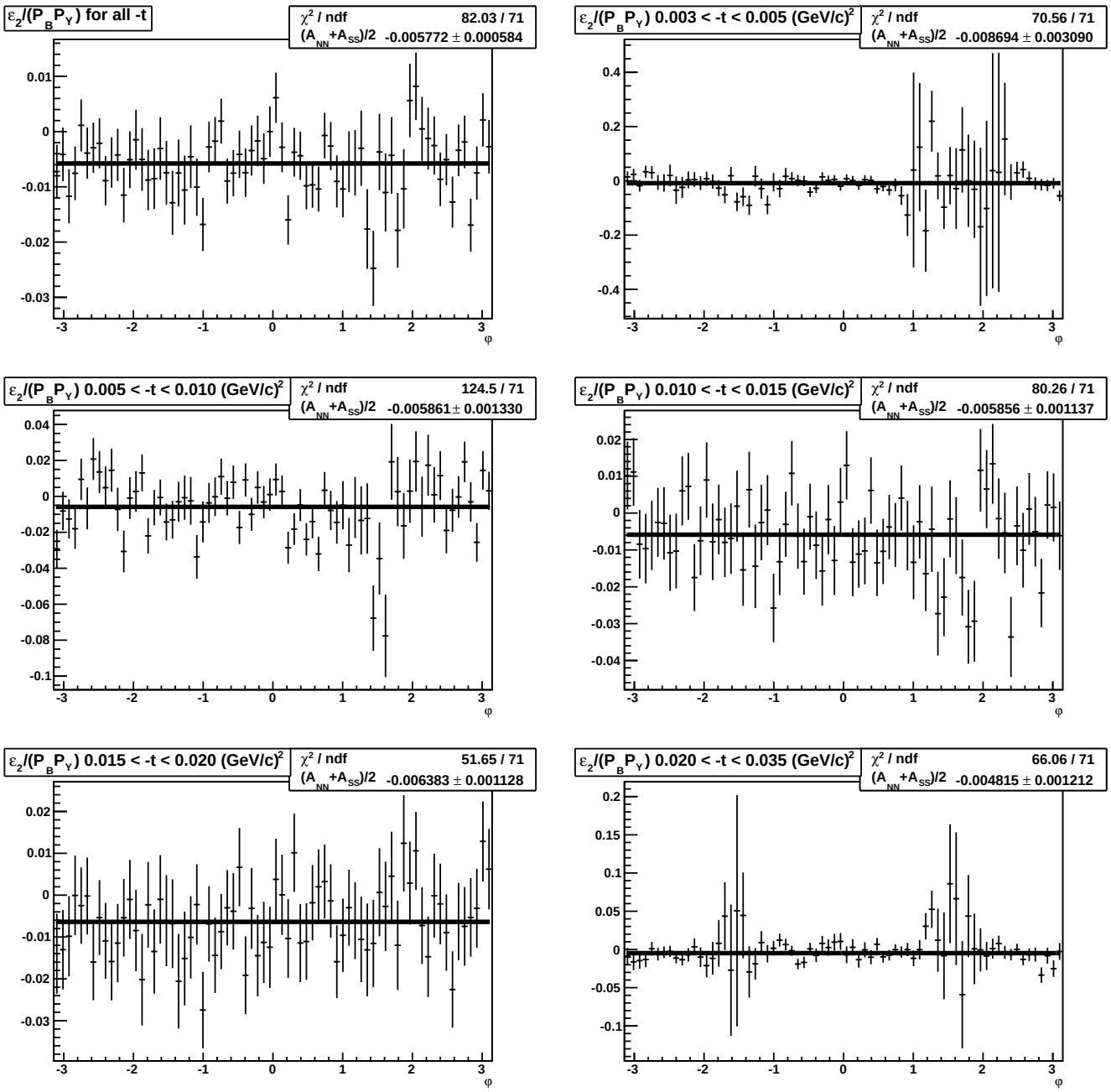

Figure 3: Fit with constatnt term $(A_{NN} + A_{SS})/2$ only. $(A_{NN} - A_{SS})/2 = 0$

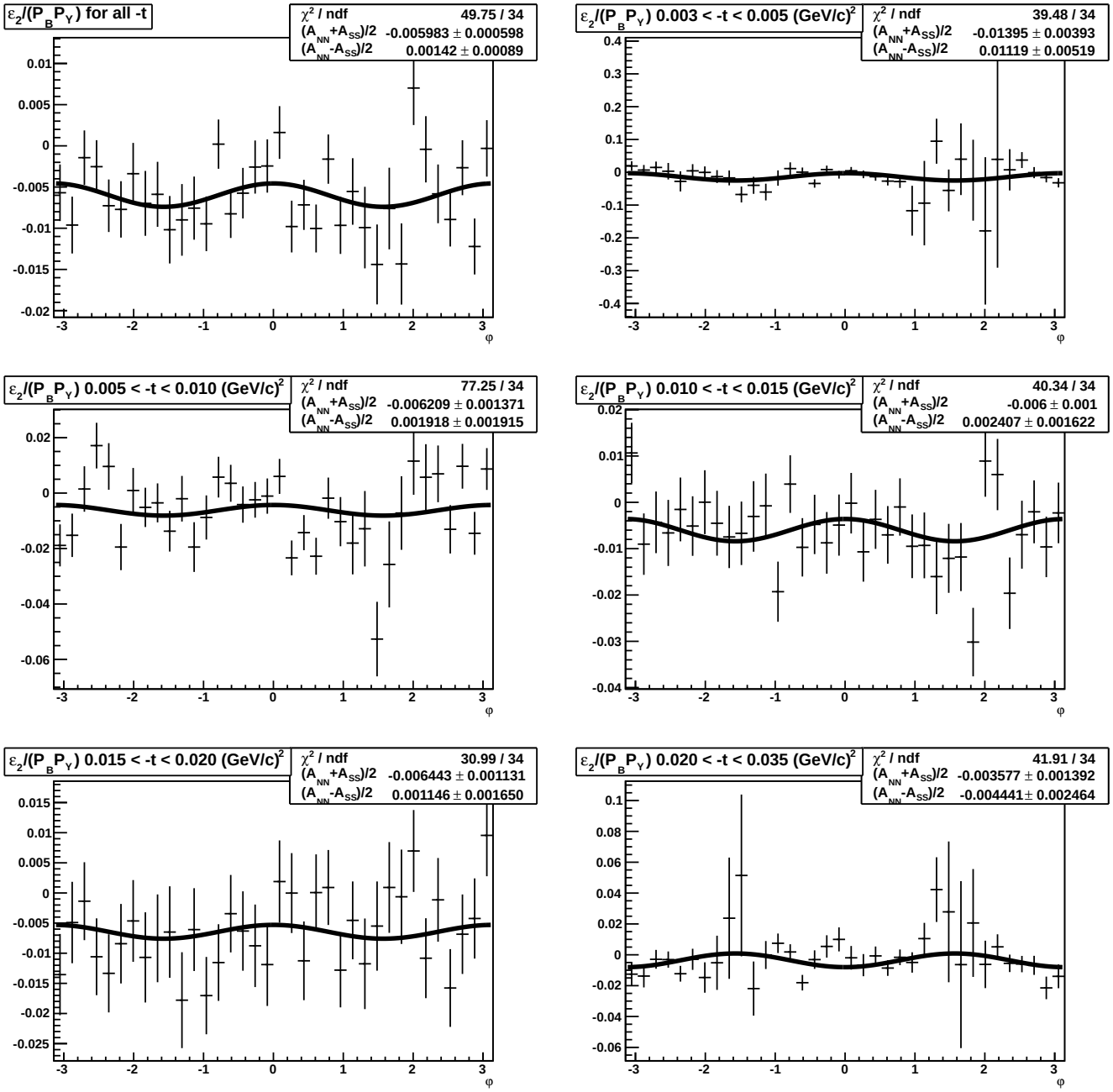

Figure 4: Fit with twice larger angular intervals

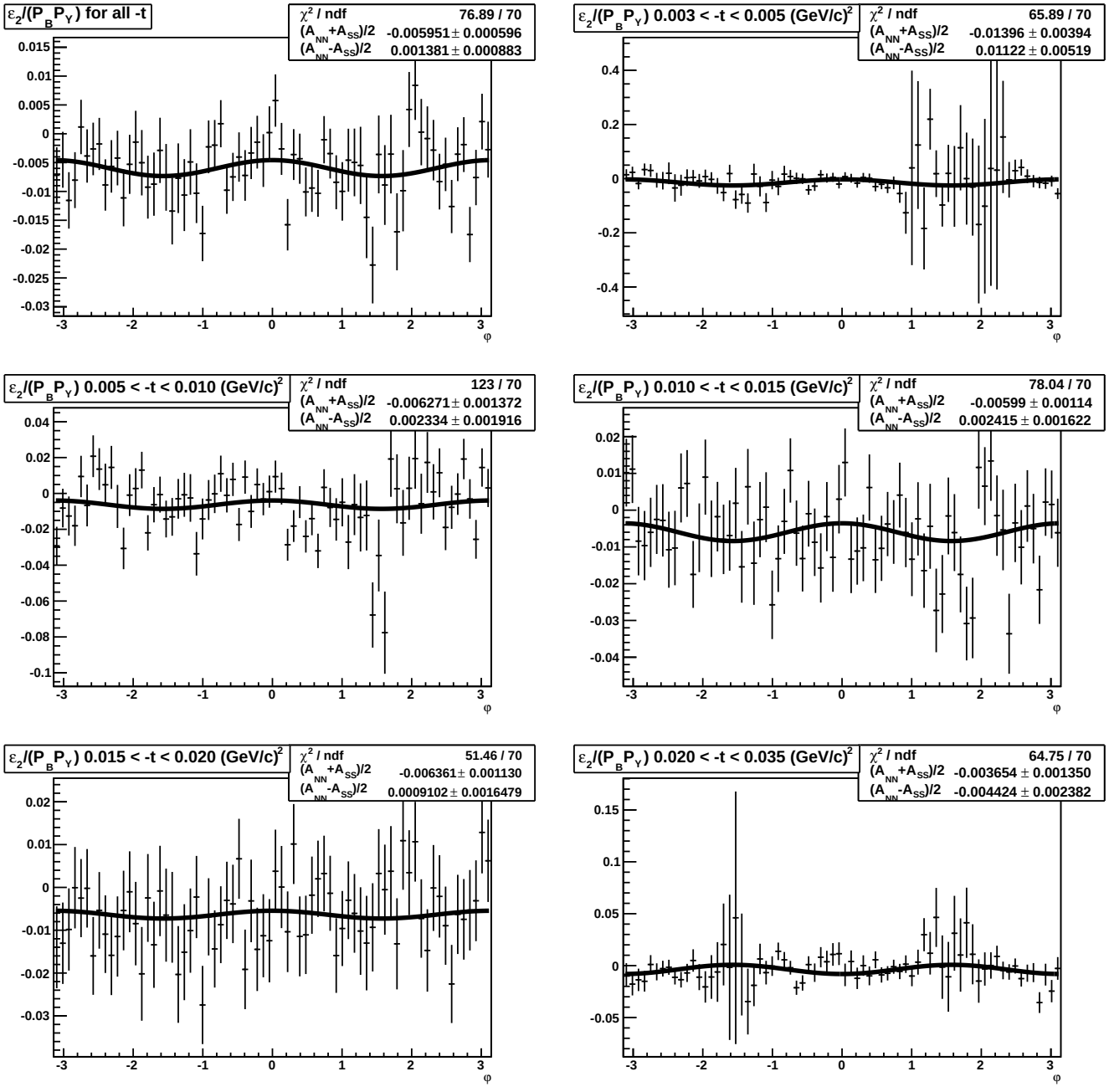

Figure 5: Fit without fiducial violume cut

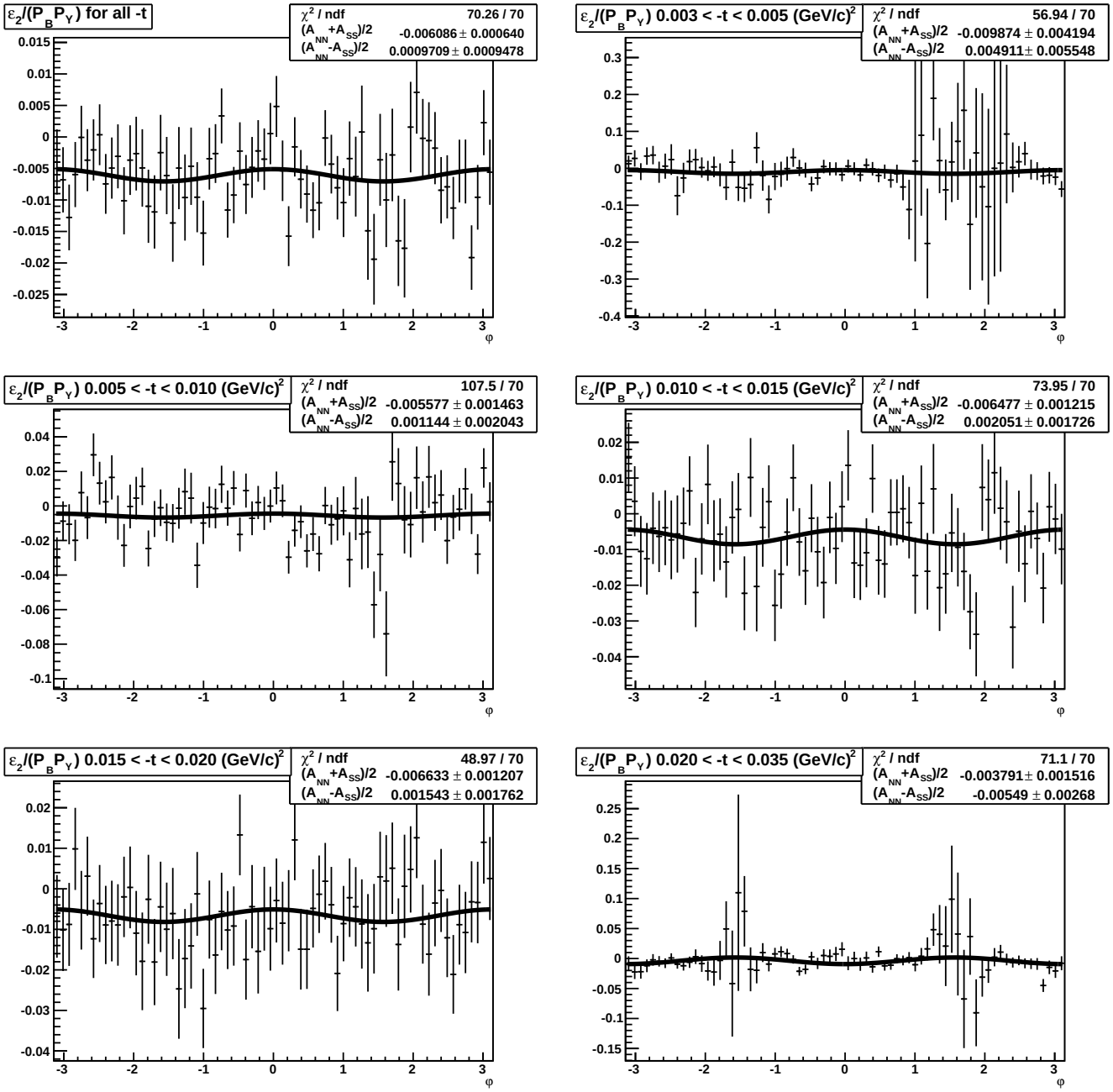

Figure 6: Fit with strong χ^2 cut: $\chi^2 < 4$

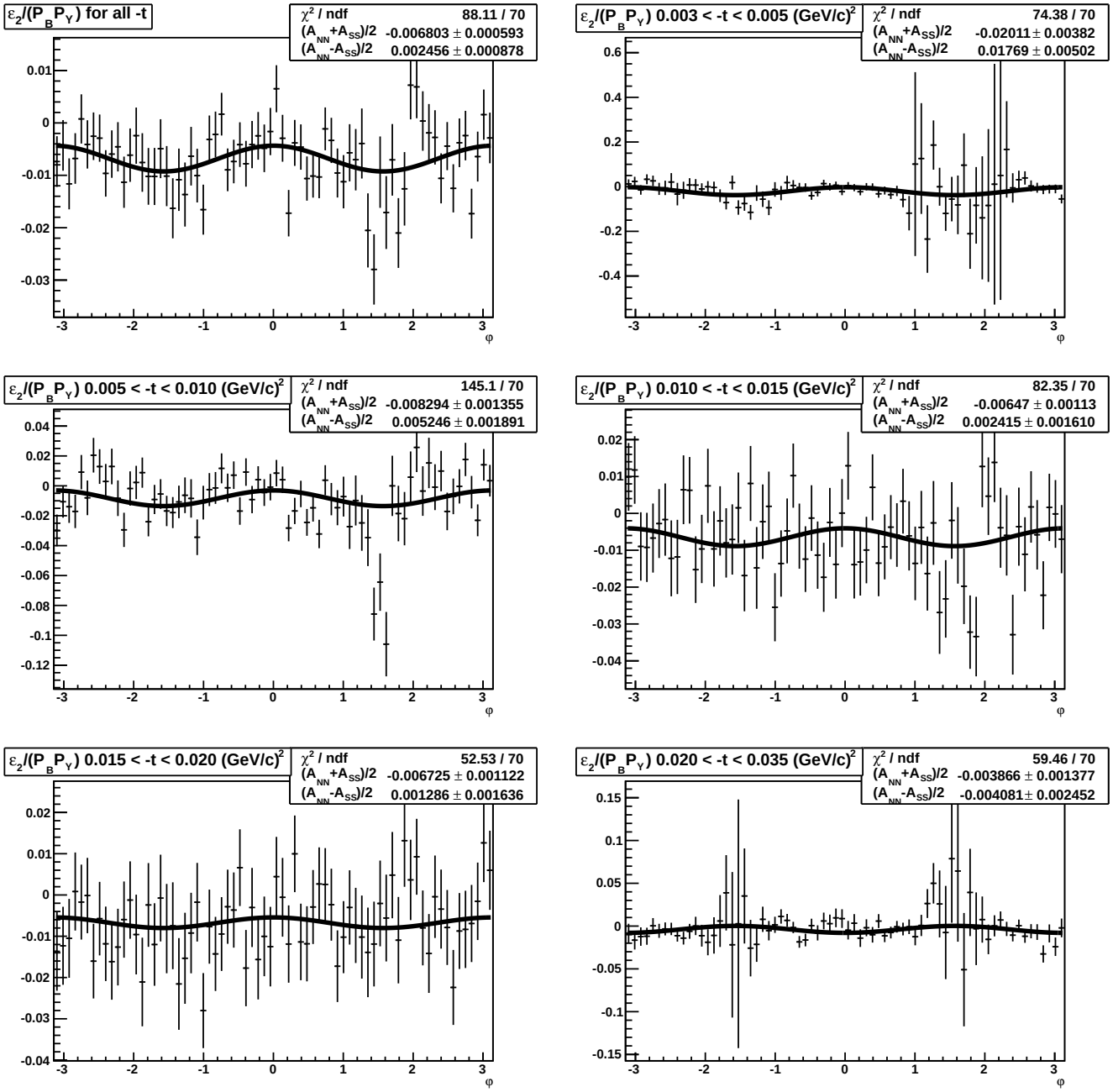

Figure 7: Fit with weak χ^2 cut: $\chi^2 < 20$

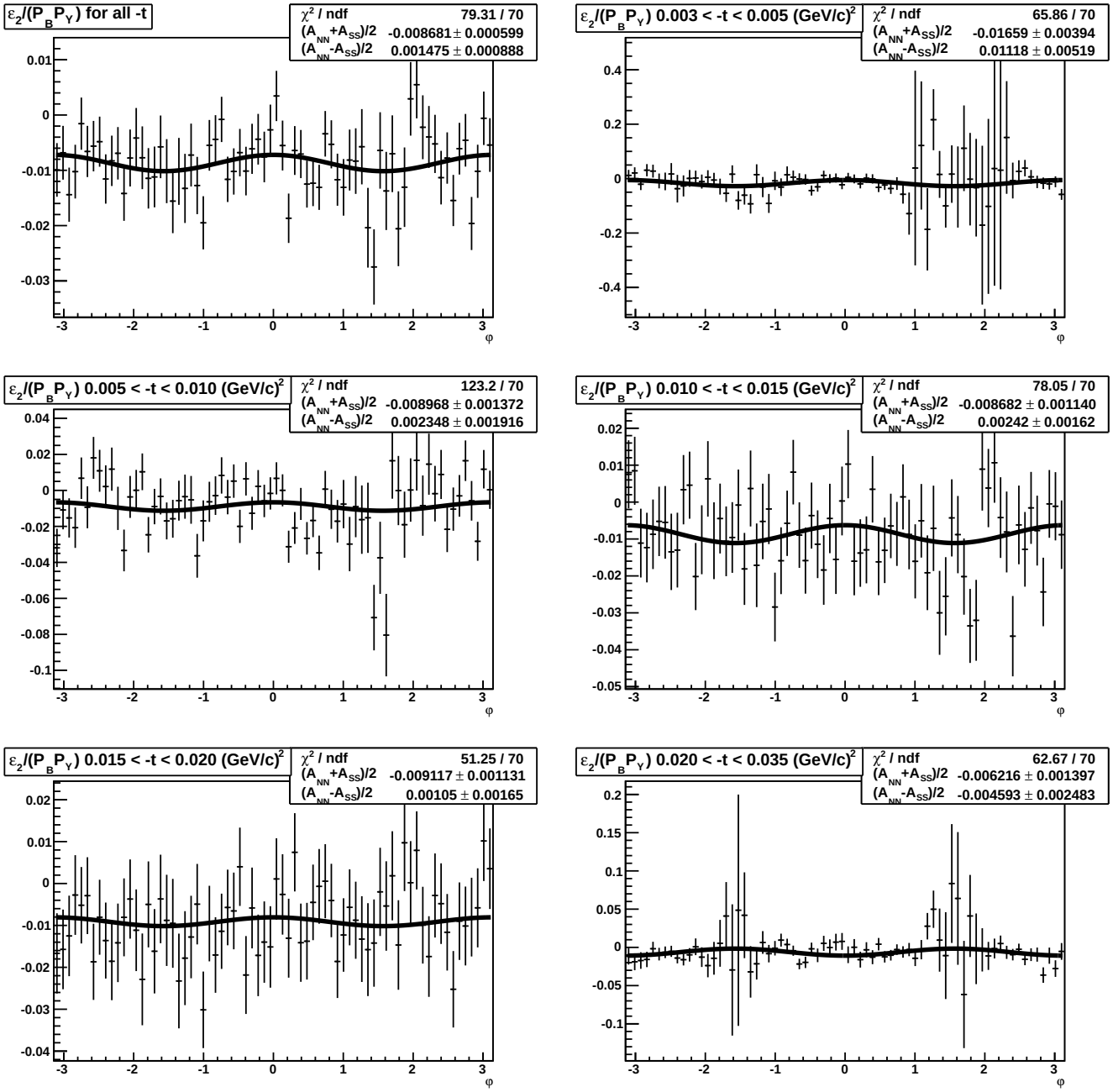

Figure 8: Fit with $\Delta R_2 = 0.0005$

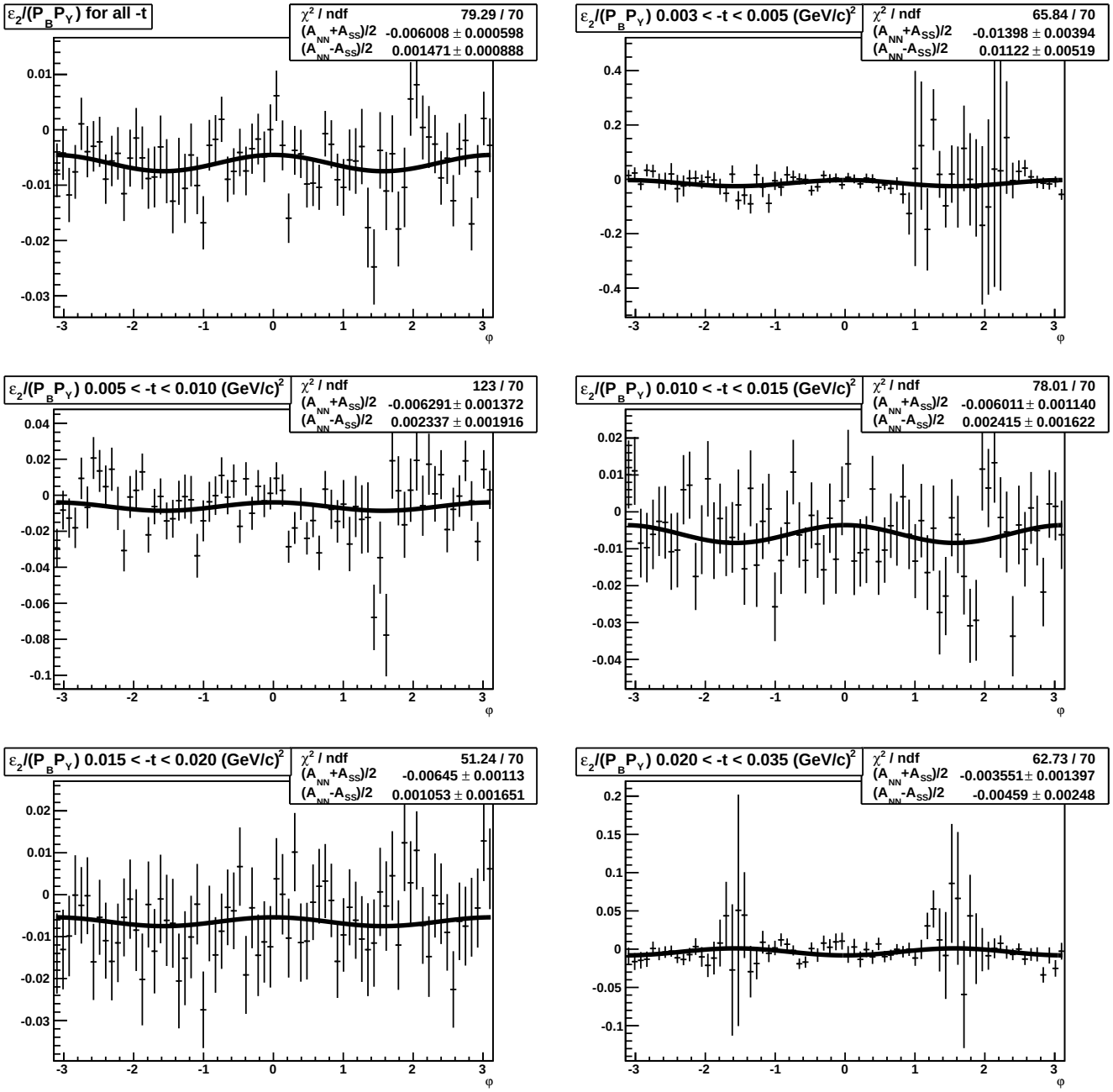

Figure 9: Fit with $\Delta R_B = 0.0005$

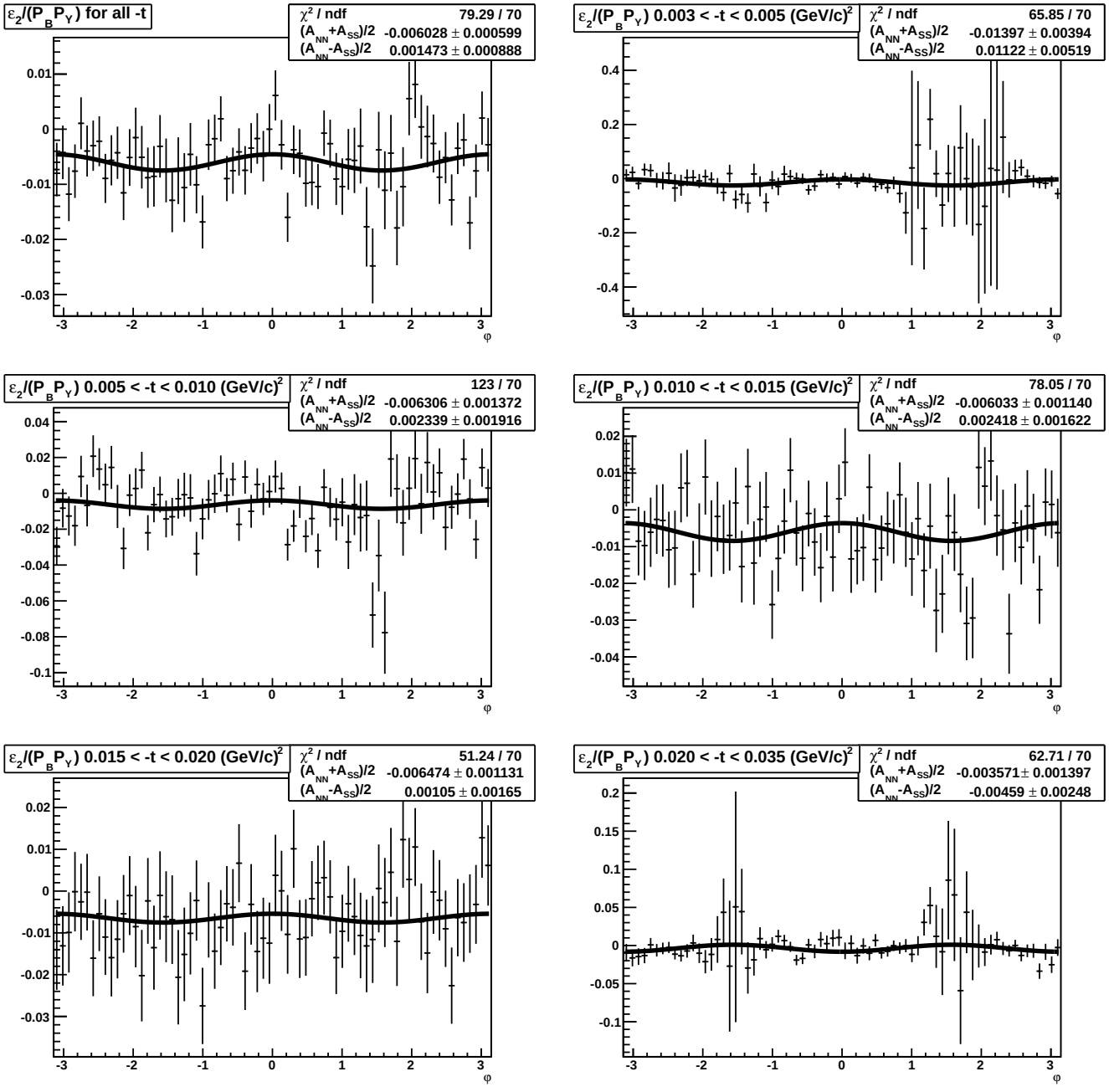

Figure 10: Fit with $\Delta R_Y = 0.0005$

4 χ^2 cut dependence and background substraction

As it was shown in the previous section, the results are rather sensitive to the value of the χ^2 cut of the elastic event selection procedure. This inspired the following careful investigation of the subject. Figures 11,12 show the dependence of the obtained double spin asymmetry values on the elastic χ^2 cut in the range $1 \leq \chi^2 \leq 30$. As in previous figures, the top left panels correspond to the average over the whole $(-t)$-range, while the following 5 panels are for the individual $(-t)$-bins. Significant behavior is seen in the first two $(-t)$-bins, and the three other dependencies are also not completely flat.

The behavior of the points at small $\chi^2 < 9$ cut values should be attributed to the statistical effects. Indeed, at these values the amount of elastic events after the cut starts to decrease significantly. This is proved by the figure 13 which presents the output of the events as a function of χ^2 cut value and its exponential fit. Thus the variations of the results can be caused by the fact that only a fraction of the statistics is used for the calculations and this region should not be used for the studies of the systematic effects.

The only thing that changes when the cut criterion is relaxed above $\chi^2 < 9$ is the amount of the background. Though the fraction of the background is very small and does not exceed several percent (below 1% in most cases), it can cause significant influence if its polarization effect is large compared to that of the elastic scattering. In this case the background subtraction procedure becomes relevant.

Commonly, the account for the background effect is made by using the formula:

$$P_{MEAS} = P_{BACKGR} \cdot \alpha + P_{ELAST} \cdot (1 - \alpha)\,, \tag{12}$$

where α is the background fraction and P's denote the polarization effects obtained from the measurement and those for the background and for the elastic process of interest, respectively.

The background fraction can be found from the χ^2 distribution of the events which is shown in figure 14. Only the lower part of the histogram is presented to concentrate on the background shape. For the χ^2 criterion defined as in [2] the theoretical shape of the distribution should be pure exponent for the elastic events, while the uniformly spread background should have flat χ^2 distribution. In our case background density seems to be slightly decreasing and is reasonably described by a linear function. Figure 14 also shows the fits with the combination of the mentioned functions. Assuming the same linear behavior of the background under the elastic peak its amount can be easily evaluated, see the first section in table 3. As for the main stream of the elastic event selection, the background fraction was defined for $\chi^2 < 9$.

Background double spin asymmetries were found using the same procedure as for the elastic events. The ragnge of $20 < \chi^2 < 60$ was chosen as the closest region to the elastic peak with nearly pure background. The fits of the raw double spin asymmetry distributions for the background events are presented in figure 15. The resulting numbers are summarized in the second section of table 3.

One can notice that the background asymmetries are really large compared to those of the elastic sacttering. Yet this is not surprising. Though large polarization effects are not expected in the physics processes which form the background, such values may arise as a result of the calculation procedure. As it was proved in [8], normalization plays the critical role as a source of systematic shifts. The selected normalization source, though very accurate for the elastic events, may have nothig in common with the background processes, which, in turn, may include beam halo or scattering on the beam gas. This explanation is fully applicable to the large values of $(A_{NN} + A_{SS})/2$, while, according to [8], $(A_{NN} - A_{SS})/2$ should not be that sensitive to the normalization. Nevertheless because of completely unknown nature of the background all the reasoning in [8] may fail.

The numbers obtained in the main stream of the analysis are listed in the third section of the table for reference. The resulting double spin asymmetries with the background effect subtracted according to (12) are presented at the bottom of table 3. Mind that formula (12) allows strict

calculations of the statistical errors according to general ruels. However because of the very small background fraction the errors of the result coincide with those before the background substraction.

The main problem of the common procedure described above in our case is in the unpredictable properties of the background. There is no guarantee that the background asymmetries observed at large χ^2 values have the same values under the elastic peak. Because of this reason another attempt was made to obtain the data free of the background effects.

As it was already mentioned, the evolution of the points in figures 11,12 can be attributed to the amount of the background inside certain cut limits. Tightening of the χ^2 cut reduces the background contribution and thus the extrapolation to $\chi^2 = 0$ means the transition to the zero background condition. Contrary to the common procedure this extrapolation method includes the effects of the background under the elastic peak.

As it was discussed the leftmost points are subject to the statistical spread, so only the region of $9 \leq \chi^2 \leq 30$ was used for the extrapolation procedure. Another reason to exclude the points at the smallest χ^2 is the following. When the cut value becomes smaller than that defined by the beam angular divergence, the periphery of the beam angular distribution starts falling out of the cut. This is especially significant for the bunches with large deviation from the average trajectory. In this case the normalization becomes invalid since it uses full average bunch intersection and thus the result may obtain unpredictable systematic shift.

According to the linear decrease of the background density with χ^2 (see fig. 14) the relevant fit function is the second order polynomial. The results of the fits are presented in figures 11,12 and the extrapolated values are summarized in table 4.

The disadvantage of the extrapolation method is that it does not give any estimate of the error of the result. While the statistical errors can be projected from the common procedure because of the similar nature of the result, the systematic uncertainty of the method itself stays undefined.

Conservative estimate of the resulting uncertainty can be made by the comparison of the two methods. The second section of table 4 present the absolute values of the difference between the results of the extrapolation method and those of the common background subtraction procedure. To form the final errors these values, treated as systematic uncertainties for indidvidual points, are added in quadratures to the statistical errors taken from the common procedure. Obtained numbers are listed at the bottom of table 4 and further on will be refered to as 'uncorrelated errors' contrary to the uncertainties from the normalization and polarization measurements which are common to all points.

The authors believe that the extrapolation method is better justified under the conditions of the experiment in comparison to the common background subtraction procedure. At the same time the uncorrelated error is overestimated to produce at least any reasonable evaluation, but no better way was invented. Because of these reasons, the final data for the publication and for the relative amplitude calculations will be taken from table 4.

Table 3: Background parameters and common subtraction procedure.

Parameter	$-t$-range, $(\mathrm{GeV/c})^2$					
	all	0.003-0.005	0.005-0.010	0.010-0.015	0.015-0.020	0.020-0.035
N_{events} for $\chi^2 < 9$	21378402	748583	4150974	5664986	5722357	4957587
Background density at $\chi^2 = 0$	12430	2546	4106	1220	1591	1696
Background slope	96.4	19.9	22.9	7.4	13.9	17.0
Background fraction α, %	**0.51**	**2.95**	**0.87**	**0.19**	**0.24**	**0.29**
Background polarization P_{BACKGR}						
$(A_{NN} + A_{SS})/2$ for $20 < \chi^2 < 60$	-0.0749 ± 0.0048	-0.0753 ± 0.0098	-0.1093 ± 0.0077	-0.0536 ± 0.0160	-0.0117 ± 0.0171	-0.0051 ± 0.0134
$(A_{NN} - A_{SS})/2$ for $20 < \chi^2 < 60$	0.0760 ± 0.0060	0.0751 ± 0.0120	0.1179 ± 0.0097	0.0585 ± 0.0220	0.0247 ± 0.0224	-0.0057 ± 0.0274
Measured polarization P_{MEAS}						
$(A_{NN} + A_{SS})/2$ for $\chi^2 < 9$	-0.0060 ± 0.0006	-0.0140 ± 0.0039	-0.0063 ± 0.0014	-0.0060 ± 0.0011	-0.0064 ± 0.0011	-0.0035 ± 0.0014
$(A_{NN} - A_{SS})/2$ for $\chi^2 < 9$	0.0015 ± 0.0009	0.0112 ± 0.0052	0.0023 ± 0.0019	0.0024 ± 0.0016	0.0011 ± 0.0017	-0.0046 ± 0.0025
Background subtracted P_{ELAST}						
$(A_{NN} + A_{SS})/2$	-0.0056 ± 0.0006	-0.0121 ± 0.0039	-0.0054 ± 0.0014	-0.0059 ± 0.0011	-0.0064 ± 0.0011	-0.0035 ± 0.0014
$(A_{NN} - A_{SS})/2$	0.0011 ± 0.0009	0.0093 ± 0.0052	0.0013 ± 0.0019	0.0023 ± 0.0016	0.0010 ± 0.0017	-0.0046 ± 0.0025

Table 4: Extrapolation results and uncorrelated error estimates

Parameter	$-t$-range, $(\mathrm{GeV/c})^2$					
	all	0.003-0.005	0.005-0.010	0.010-0.015	0.015-0.020	0.020-0.035
Extrapolation to $\chi^2 = 0$						
$(A_{NN} + A_{SS})/2$	-0.0051	-0.0070	-0.0043	-0.0052	-0.0059	-0.0028
$(A_{NN} - A_{SS})/2$	0.0005	0.0048	-0.0005	0.0025	0.0008	-0.0054
$\delta^{extrapol}_{(A_{NN}+A_{SS})/2}$	0.0005	0.0051	0.0011	0.0007	0.0005	0.0007
$\delta^{extrapol}_{(A_{NN}-A_{SS})/2}$	0.0006	0.0045	0.0018	0.0002	0.0002	0.0008
$\delta^{uncor}_{(A_{NN}+A_{SS})/2}$	0.0008	0.0064	0.0018	0.0013	0.0012	0.0016
$\delta^{uncor}_{(A_{NN}-A_{SS})/2}$	0.0011	0.0069	0.0026	0.0016	0.0017	0.0026

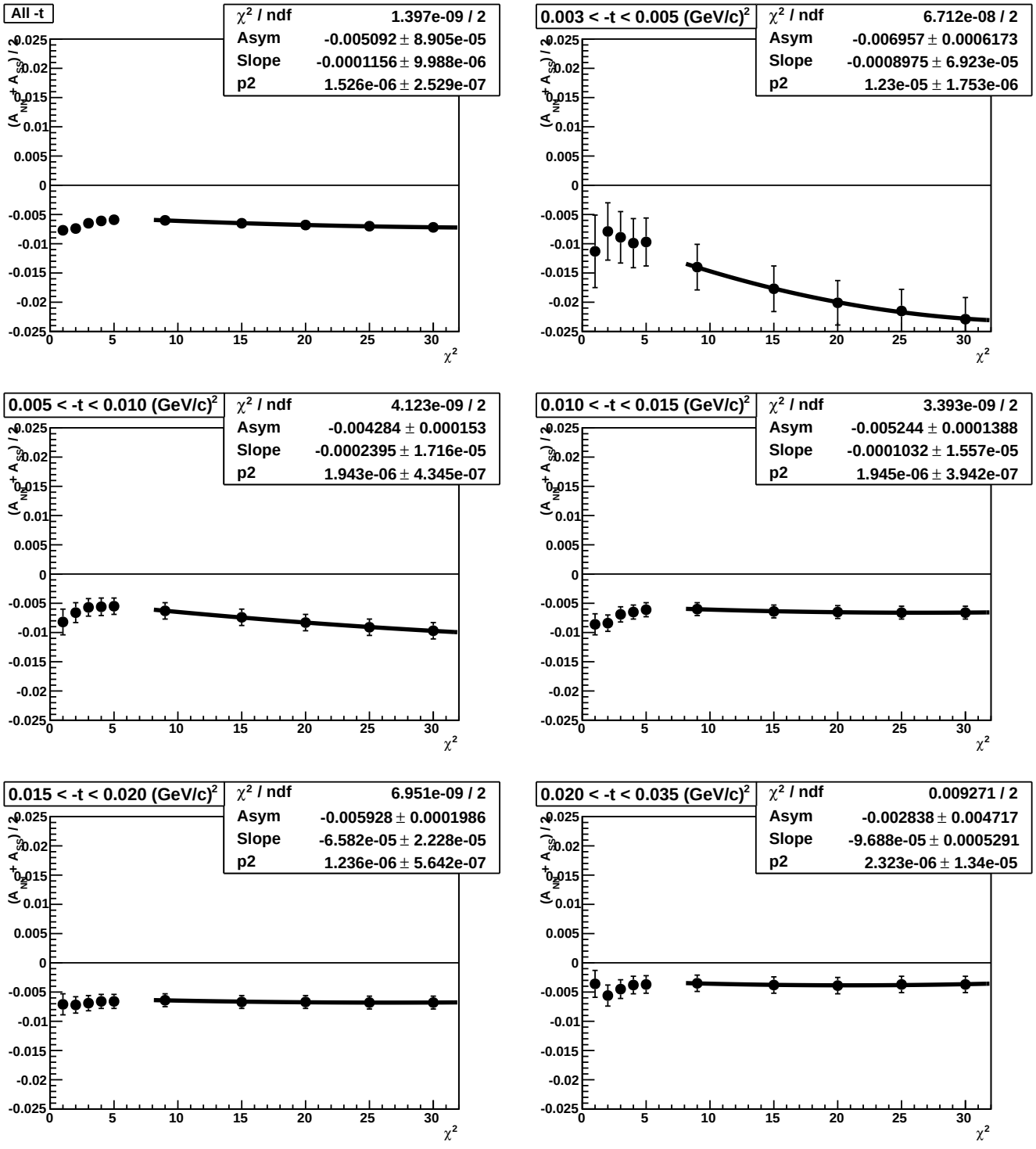

Figure 11: χ^2-cut dependence for $(A_{NN} + A_{SS})/2$ and its quadratic fit to $\chi^2 \to 0$.

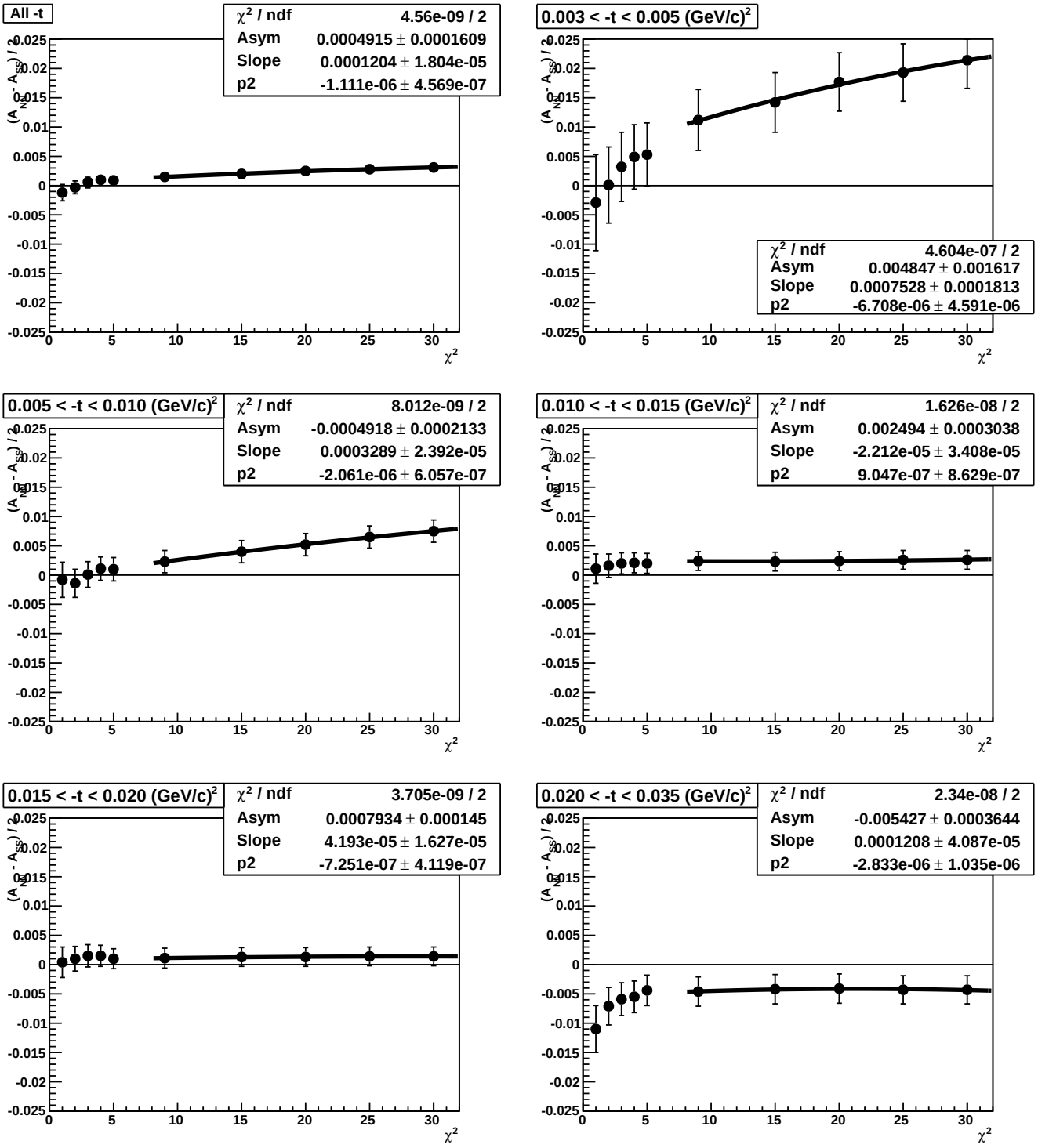

Figure 12: χ^2-cut dependence for $(A_{NN} - A_{SS})/2$ and its quadratic fit to $\chi^2 \to 0$.

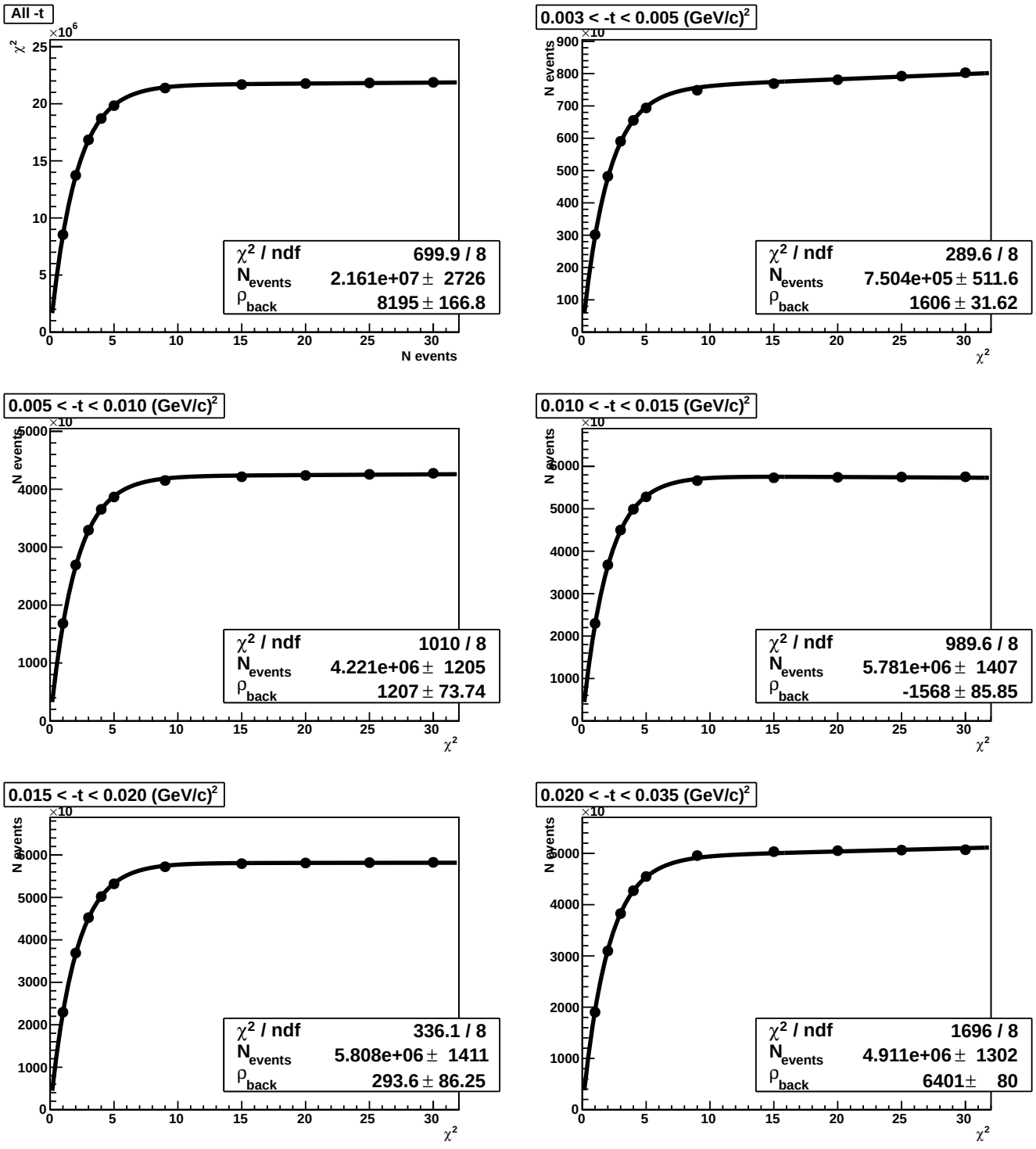

Figure 13: Event output as a function of the χ^2 cut.

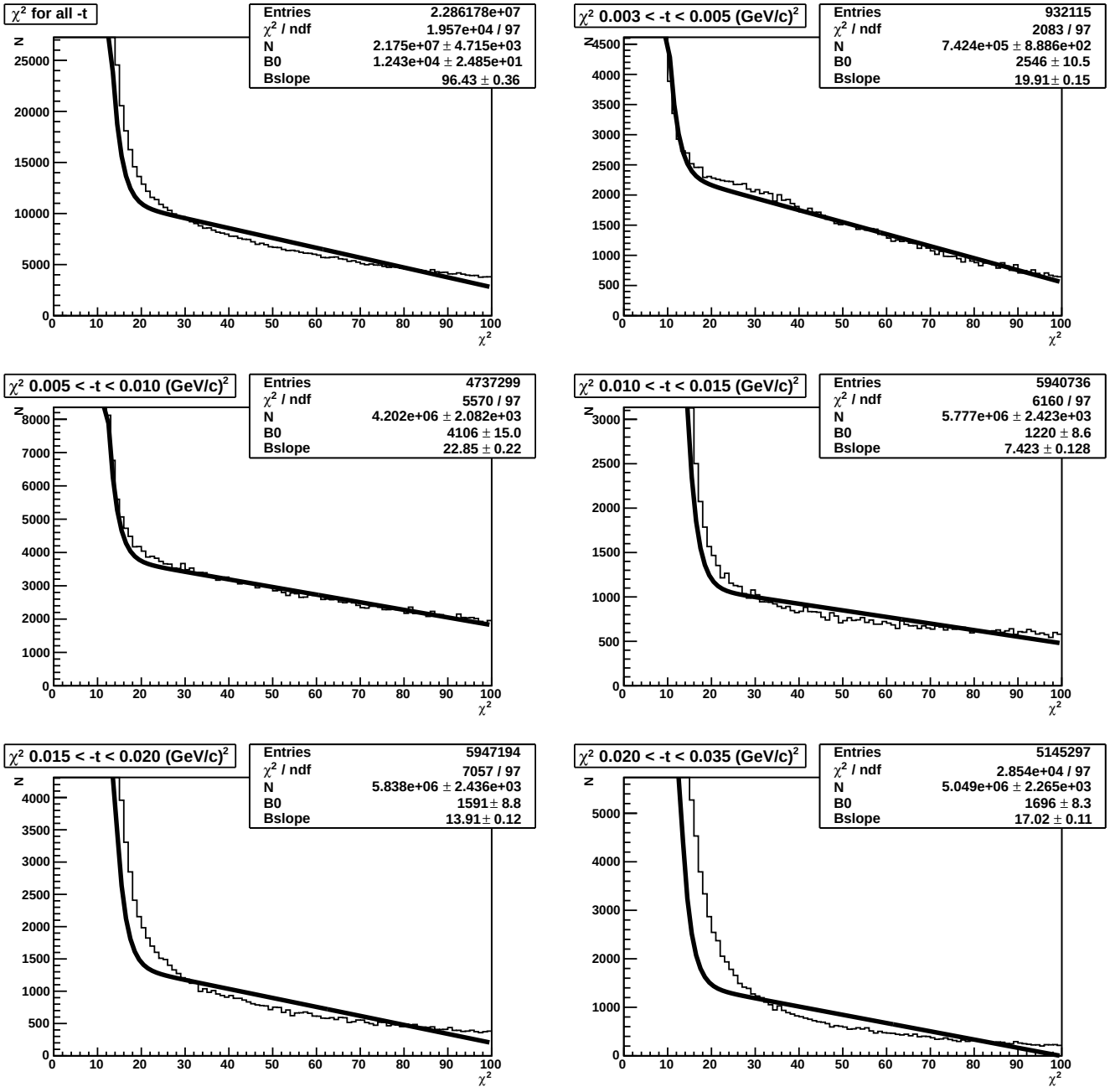

Figure 14: χ^2 distribution of the events and its fit with the exponent with linear background.

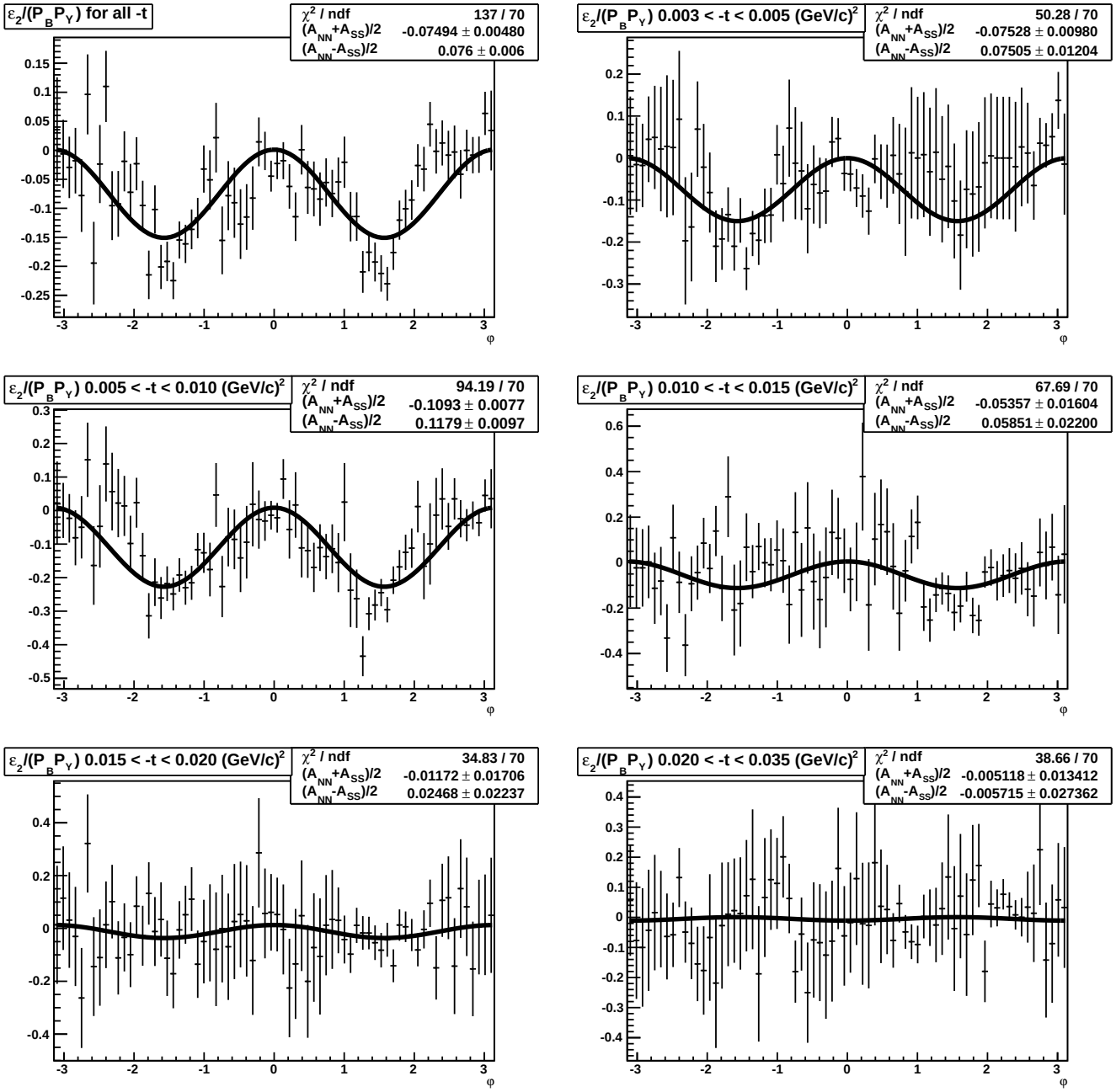

Figure 15: Raw double spin asymmetry of the background.

5 Relative amplitudes r_2 and r_4

The results obtained for each of 5 $(-t)$-ranges of the experiment are plotted in figure 16. All points of $(A_{NN} - A_{SS})/2$ (bottom panel) do not deviate from zero more than by two standard errors and the deviations are of different signs. The average is well compatible with zero. However slight negative slope can be imagined in the $(-t)$ dependence of the data, but it's difficult to state that it bears any physics meaning. On the contrary, $(A_{NN} + A_{SS})/2$ (top panel) is significantly below zero and the absolute values are of the order of $5 \cdot 10^{-3}$. The distribution is approximately flat and the average is more than 6 standard deviations from zero. The normalization error of $8.4 \cdot 10^{-4}$ (see [8]) is illustrated by the bar at the bottom of the panel. Even taking it into account the data can not be made compatible with zero.

The fits to extract the relative amplitudes r_2 and r_4 were made using full set of exact formulas (A.13–A.27). The theoretical constants and world averages were taken similarly to [2]. The value of r_5, though it doesn't introduce any significant influence, was taken also from [2]. It is obvious from approximate expressions (A.30,A.31) that $(A_{NN} + A_{SS})/2$ is mainly defined by r_2 and is basically independent on r_4, while, on the contrary, $(A_{NN} - A_{SS})/2$ is sensitive to r_4 and is not influenced by r_2.

Two separate fits of the double spin asymmetries were made to the data in figure 16 using successive approximation. The fixed value of r_2 from the fit of $(A_{NN} + A_{SS})/2$ was substituted to obtain r_4 from $(A_{NN} - A_{SS})/2$ and vice versa. The process converges already after the second step, which is natural because of (A.30,A.31).

The results of the fit are summarized in the table 5. Nondiagonal elements of the covariance matrices, necessary for the confidence ellipse calculations, are also listed in the last column.

Table 5: r_2 and r_4 fit results with uncorrelated errors only

Parameter	Re	Im	σ^2_{Re}	σ^2_{Im}	cov(Re, Im)
r_2	0.00216	-0.00257	$5.758 \cdot 10^{-5}$	$1.486 \cdot 10^{-7}$	$-1.155 \cdot 10^{-6}$
r_4	3.51	-0.122	4.075	0.009123	-0.1574

To obtain the full error on the relative amplitude values, their numerical derivatives on the beam polarization product and normalization ratio R_2 (see [8]) were calculated according to appendix B. Figure 17 illustrates this process. In the top and the middle panels the fits were made to the data, calculated with the beam polarization product shifted by its standard deviation. As polarization only scales the effect which is already very small the contribution of polarization error to the systematic error is also small. So instead of accurate averaging of (10) the simplified expression was used which assumes equal fill statistics:

$$\frac{\delta(P_B \cdot P_Y)}{P_B \cdot P_Y} = \sqrt{\frac{1}{4}\sum_{i=1}^{4}((\frac{\delta P_B^i}{P_B^i})^2 + (\frac{\delta P_Y^i}{P_Y^i})^2) + \delta^2_{GLOB}} = 0.14\,. \tag{13}$$

The bottom panel of figure 17 shows the fit of $(A_{NN} + A_{SS})/2$ with the double spin normalization ratio R_2 [8] shifted by its uncertainty $\delta R_2 = 1.56 \cdot 10^4$. As it was proved in the refered note, no other normalization uncertainty produce noticeable systematic error in the double spin asymmetries, while $(A_{NN} - A_{SS})/2$ is not even influenced by R_2. The shifts of the relative amplitudes caused by the 1-σ disturbance of the contributing parameters are presented in table 6.

In accordance to appendix B the following formula was used for the final error matrix calculations:

$$M_{ij} = \begin{pmatrix} \sigma^2_{\mathrm{Re}} & \mathrm{cov(Re,Im)} \\ \mathrm{cov(Re,Im)} & \sigma^2_{\mathrm{Im}} \end{pmatrix} + \begin{pmatrix} (\Delta^P_{\mathrm{Re}})^2 & \Delta^P_{\mathrm{Re}}\Delta^P_{\mathrm{Im}} \\ \Delta^P_{\mathrm{Re}}\Delta^P_{\mathrm{Im}} & (\Delta^P_{\mathrm{Im}})^2 \end{pmatrix} + \begin{pmatrix} (\Delta^N_{\mathrm{Re}})^2 & \Delta^N_{\mathrm{Re}}\Delta^N_{\mathrm{Im}} \\ \Delta^N_{\mathrm{Re}}\Delta^N_{\mathrm{Im}} & (\Delta^N_{\mathrm{Im}})^2 \end{pmatrix}, \tag{14}$$

Table 6: r_2 and r_4 shifts by polarization product (P) and normalization (N) errors

Parameter	Re	Im
$\Delta^P(r_2)$	0.00030	-0.00035
$\Delta^P(r_4)$	0.505	-0.019
$\Delta^N(r_2)$	-0.00001	0.00042

where the first term is taken from table 5 and the two others come from table 6. Mind that in case of r_4 the last matrix is zero.

The resulting ellipses for the confidence level of one standard deviation are shown in figure 18 for r_2 (top) and r_4 (bottom). Red shapes represent the uncorrelated error only, green and blue lines are the degenerated ellipses for the error matrices of the polarization product and normalization, respectively, while the black curves reflect the full error matrices according to (14). The corresponding numbers are presented in table 7.

Table 7: r_2 and r_4 final results and error matrix elements

Parameter	Re	Im	cov(Re, Im)
r_2	0.0022 ± 0.0076	-0.00257 ± 0.00067	$-1.26 \cdot 10^{-6}$
r_4	3.51 ± 2.08	-0.122 ± 0.097	-0.167

The real part of r_2 is well consistent with zero and is influenced neither by the polarization nor by the normalization errors. At the same time, $\mathrm{Im}\, r_2$, though has a very small negative value, is away from zero by about 3.7σ in spite of the fact that the main contribution from the common errors goes into this imaginary part. The two components of r_2 are not highly correlated (the ellipse is basically horizontal), and thus a good estimate on $\mathrm{Im}\, r_2$ is obtained. Yet $\mathrm{Re}\, r_2$ has a large error and is not very well constrained.

r_4 makes quite a different story. Though points of $(A_{NN} - A_{SS})/2$ make a good average of zero and their $(-t)$ behavior is very tiny, if observable at all, the formal fitting procedure in figure 16 gives the numbers, which deviate from zero by 1.7 and 1.2 of the corresponding total errors in real and imaginary parts. The polarization product uncertainty is negligible compared to that out of the formal fit and only slightly increases the errors on both of the components. It is worth mentioning that the huge mean value of $\mathrm{Re}\, r_4$ is not surprising by itself because of the structure of (A.31). Indeed, the kinematic factor t/m^2 is taken out of the term containing r_4. The value of this factor is very small in the kinematic region of the experiment ($0.005 < t/m^2 < 0.03$) and thus even small asymmetries may formally produce very large numbers of r_4.

The double spin flip amplitude ϕ_4 is supposed to be much smaller than dominating ϕ_+. In the $(-t)$ range of the experiment, because of the factor t/m^2, the ratio ϕ_4/ϕ_+ stays in an range of $(0.02 < \phi_4/\phi_+ < 0.1)$ even with such a value of $|r_4| \sim 3$. This might be considered a little too large, but not fully incredible. However, at $(-t)$ above the experiment range, this ratio would grow unreasonably high. Thus the mean values formally obtained for the components of r_4 can not be treated as physically meaningful.

Meanwhile, the hypothesis of $r_4 \sim 0$ is not too bad. The curve with r_4 fixed at 0 is presented in figure 16 as a dashed blue line. All other 'ingredients' are fixed at the same values as in the main fit. The numerical value of this fit $\chi^2 = 7.36/5\,\mathrm{d.f.}$ (shown in blue at the bottom) is not too high to reject the hypothesis. This conclusion is in correspondence with the r_4 image in figure 18 (bottom):

it is obvious that the point (0,0) will fall inside the 2σ ellipse, while if one draws an ellipse going through 0, it will designate a confidence level of about 85%. According to general statistical rules this is not enough to state that the obtained value is different from 0.

The authors think that the whole procedure of the data analysis is carried out as thoroughly as possible and is well justified at every step. The results obtained for the relative amplitude r_2 are reliable at the level of the estimated uncertainty. At the same time the numbers for r_4, though formally differ from zero, should not be considered as any reasonable constraint for this amplitude. A better estimate of r_4 might be obtained from the data of this experimant if some model relation between its real and imaginary parts is assumed. Unfortunately the authors didn't find any mention of such relation in the literature.

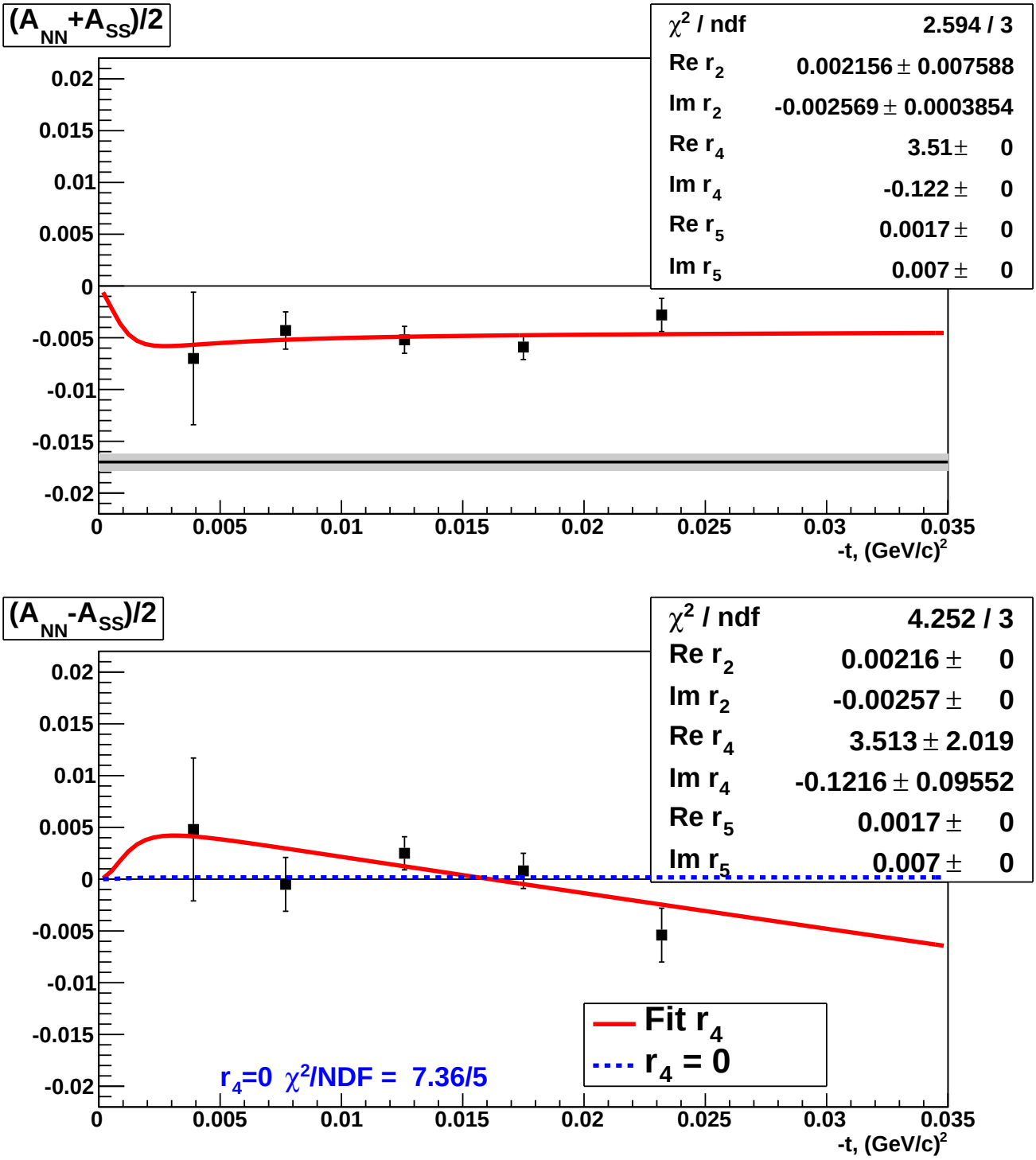

Figure 16: Results on $(A_{NN}+A_{SS})/2$ (top) and $(A_{NN}-A_{SS})/2$ (bottom). Uncorrelated errors only. Fits for r_2 and r_4.

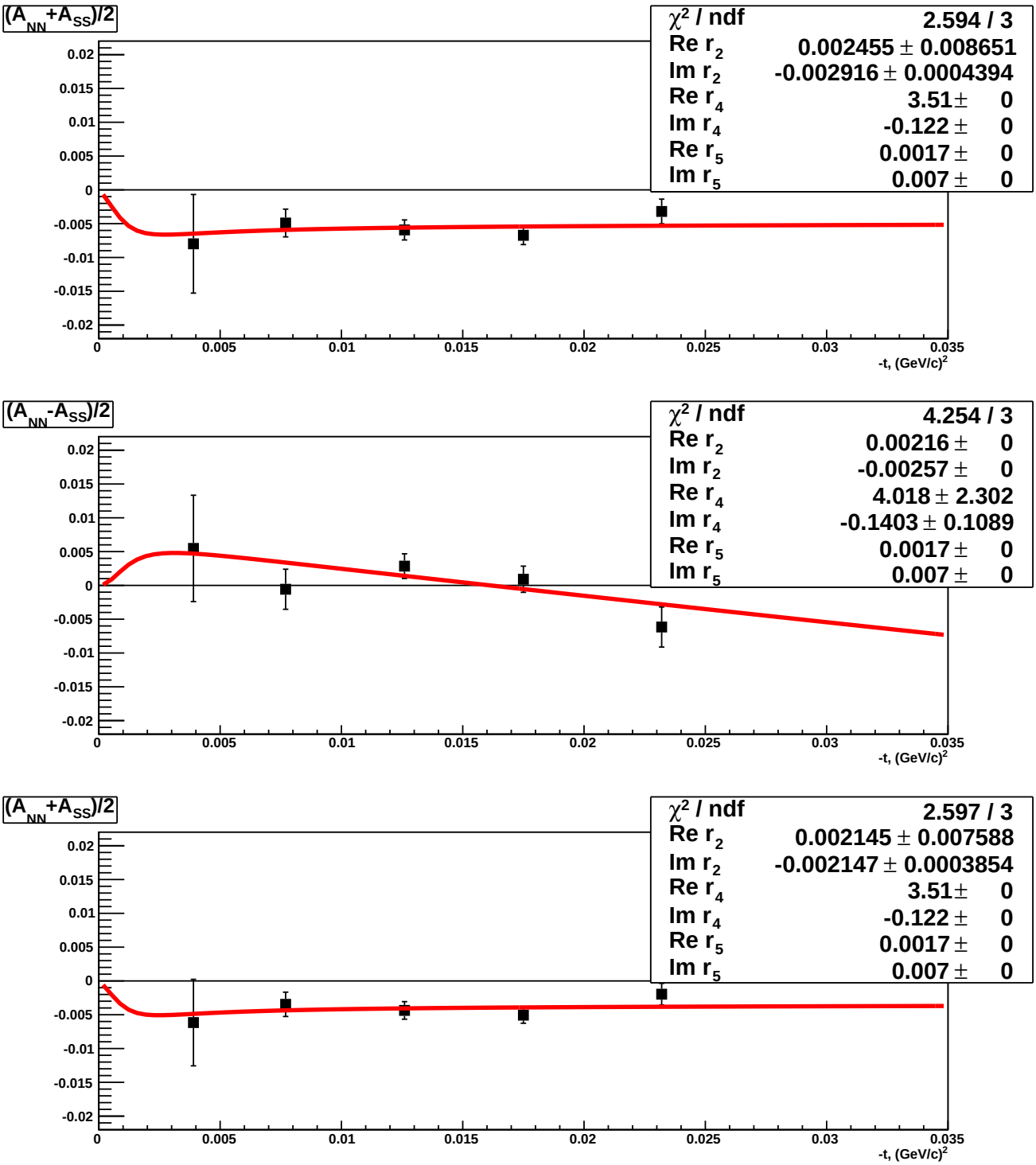

Figure 17: Fit for r_2 and r_4 with polarization one-σ-shifted (top two figures) and normalization one-σ-shifted (bottom figure)

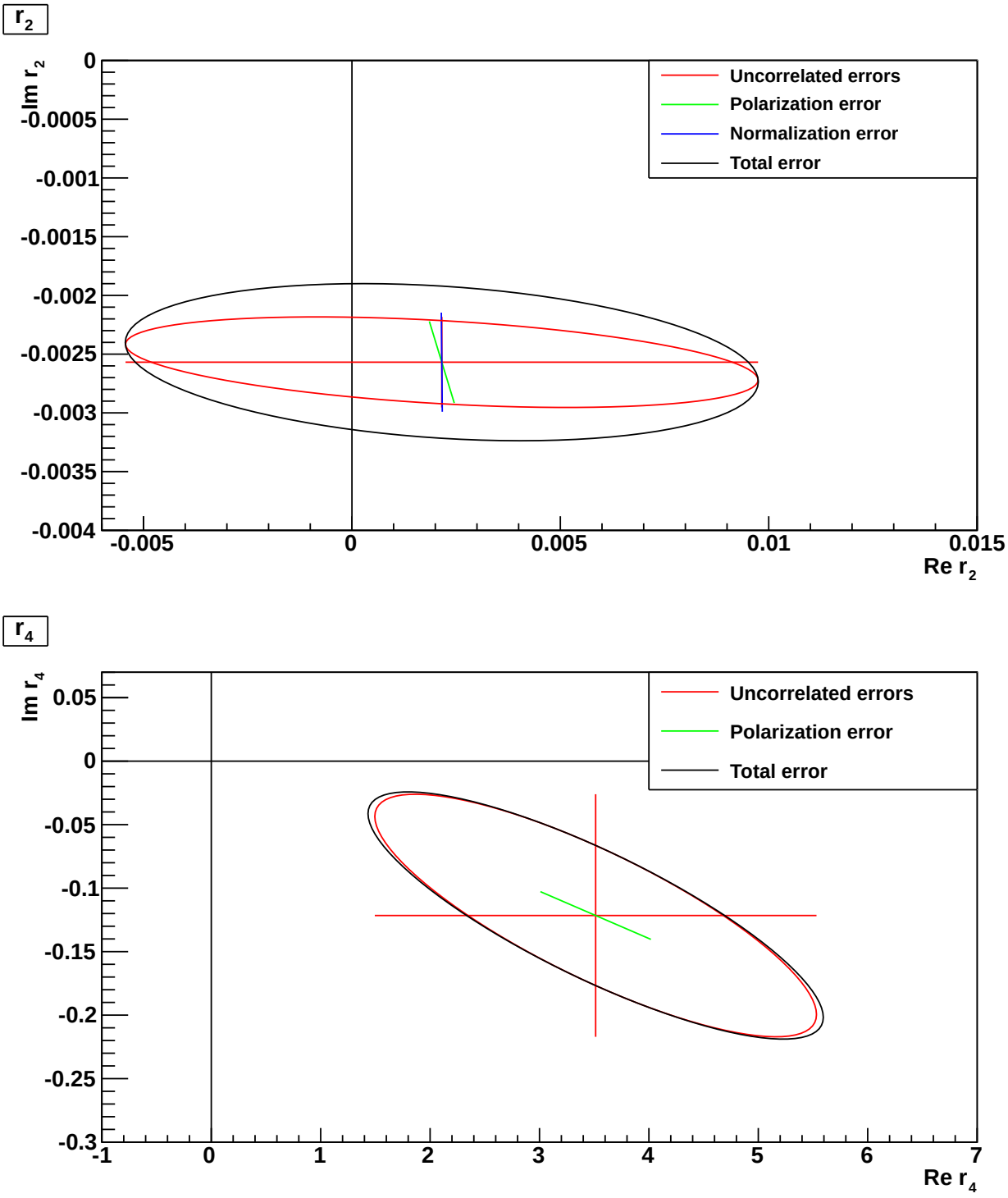

Figure 18: r_2 and r_4 one-*sigma* confidence ellipses

A Amplitudes and double spin asymmetries

We will start with standard definition of the 5 independent helicity amplitudes describing proton-proton elastic scattering [3, 1, 10]:

$$\begin{aligned}
\phi_1(s,t) &= <++|M|++>, && \text{(A.1)}\\
\phi_2(s,t) &= <++|M|-->, && \text{(A.2)}\\
\phi_3(s,t) &= <+-|M|+->, && \text{(A.3)}\\
\phi_4(s,t) &= <+-|M|-+>, && \text{(A.4)}\\
\phi_5(s,t) &= <++|M|+->\ . && \text{(A.5)}
\end{aligned}$$

Observables are expressed in the terms of amplitudes as [3]:

$$\begin{aligned}
\sigma_{tot} &= \frac{4\pi}{s}\mathrm{Im}\,(\phi_1(s,t)+\phi_3(s,t))|_{t=0}\,, && \text{(A.6)}\\
\frac{d\sigma}{dt} &= \frac{2\pi}{s^2}\{|\phi_1|^2+|\phi_2|^2+|\phi_3|^2+|\phi_4|^2+4|\phi_5|^2\}\,, && \text{(A.7)}\\
A_N\frac{d\sigma}{dt} &= -\frac{4\pi}{s^2}\mathrm{Im}\,\{\phi_5^*(\phi_1+\phi_2+\phi_3-\phi_4)\}\,, && \text{(A.8)}\\
A_{NN}\frac{d\sigma}{dt} &= \frac{4\pi}{s^2}\{2|\phi_5|^2+\mathrm{Re}\,(\phi_1^*\phi_2-\phi_3^*\phi_4)\}\,, && \text{(A.9)}\\
A_{SS}\frac{d\sigma}{dt} &= \frac{4\pi}{s^2}\{\mathrm{Re}\,(\phi_1^*\phi_2+\phi_3^*\phi_4)\}\,, && \text{(A.10)}\\
A_{SL}\frac{d\sigma}{dt} &= \frac{4\pi}{s^2}\mathrm{Re}\,\{\phi_5^*(\phi_1+\phi_2-\phi_3+\phi_4)\}\,, && \text{(A.11)}\\
A_{LL}\frac{d\sigma}{dt} &= \frac{2\pi}{s^2}\{|\phi_1|^2+|\phi_2|^2-|\phi_3|^2-|\phi_4|^2\}\,, && \text{(A.12)}\\
\frac{A_{NN}+A_{SS}}{2}\frac{d\sigma}{dt} &= \frac{4\pi}{s^2}\{|\phi_5|^2+\mathrm{Re}\,(\phi_1^*\phi_2)\}\,, && \text{(A.13)}\\
\frac{A_{NN}-A_{SS}}{2}\frac{d\sigma}{dt} &= \frac{4\pi}{s^2}\{|\phi_5|^2-\mathrm{Re}\,(\phi_3^*\phi_4)\}\,. && \text{(A.14)}
\end{aligned}$$

Each of the amplitudes can be presented as a sum of hadron and electromagnetic parts:

$$\phi_i(s,t)=\phi_i^H(s,t)+e^{i\delta(s,t)}\phi_i^{EM}(s,t)\,, \qquad \text{(A.15)}$$

where $\delta(s,t)$ is approximately independent of helisity Coulomb phase [1, 11]:

$$\delta(s,t)=\alpha(ln\frac{-2}{t(B(s)+8/\Lambda^2)}-\gamma)\,, \qquad \text{(A.16)}$$

where α is the fine-structure constant, $B(s)$ — slope parameter of the diffraction cone, $\gamma=0.5772...$ — Euler's constant and $\Lambda^2=0.71$ GeV^2. We will omit superscript ^{H} below.

We will introduce usual definition of $\phi_+=(\phi_1+\phi_3)/2$, $\rho=\mathrm{Re}\,\phi_+/\mathrm{Im}\,\phi_+$ and of relative amplitudes r_i assuming that r_i are independent of t in our range:

$$\phi_2=2r_2\mathrm{Im}\,\phi_+\ \ ,\ \ \phi_4=\frac{-t}{m^2}r_4\mathrm{Im}\,\phi_+\ \text{ and }\ \phi_5=\frac{\sqrt{-t}}{m}r_5\mathrm{Im}\,\phi_+\,. \qquad \text{(A.17)}$$

From the optical theorem (A.6) we have:

$$\phi_+(s,t) = (\rho+i)\frac{s\sigma_{tot}}{8\pi}e^{Bt/2}\approx(\rho+i)\frac{s\sigma_{tot}}{8\pi}\,, \qquad \text{(A.18)}$$

$$\phi_2(s,t) = r_2\frac{s\sigma_{tot}}{4\pi}e^{Bt/2} \approx r_2\frac{s\sigma_{tot}}{4\pi}\,, \tag{A.19}$$

$$\phi_4(s,t) = r_4\frac{-ts\sigma_{tot}}{8\pi m^2}e^{Bt/2} \approx -r_4\frac{ts\sigma_{tot}}{8\pi m^2}\,, \tag{A.20}$$

$$\phi_5(s,t) = r_5\frac{\sqrt{-t}s\sigma_{tot}}{8\pi m}e^{Bt/2} \approx r_5\frac{\sqrt{-t}s\sigma_{tot}}{8\pi m}\,. \tag{A.21}$$

We will assume $\phi_1 \approx \phi_3 \approx \phi_+$.

For small t Coulomb amplitudes are written as [3]:

$$\phi_1^{EM} = \phi_3^{EM} = \phi_+^{EM} = \frac{\alpha s}{t}F_1^2 \approx \frac{\alpha s}{t} = -\frac{\sigma_{tot}s}{8\pi}\frac{t_c}{t}\,, \tag{A.22}$$

$$\phi_2^{EM} = -\phi_4^{EM} = \frac{\alpha s(\mu-1)^2}{4m^2}F_2^2 \approx \frac{\alpha s(\mu-1)^2}{4m^2} = -\frac{\sigma_{tot}s(\mu-1)^2}{32\pi}\frac{t_c}{m^2}\,, \tag{A.23}$$

$$\phi_5^{EM} = -\frac{\alpha s(\mu-1)}{2m\sqrt{-t}}F_1F_2 \approx -\frac{\alpha s(\mu-1)}{2m\sqrt{-t}} = \frac{\sigma_{tot}s(\mu-1)}{16\pi}\frac{t_c}{m\sqrt{-t}}\,, \tag{A.24}$$

where μ is magnetic moment of a proton, $t_c = -8\pi\alpha/\sigma_{tot}$, F_1 and F_2 are electromagnetic formfactors:

$$F_1 = \frac{1-\mu\frac{t}{4m^2}}{(1-\frac{t}{4m^2})(1-\frac{t}{\Lambda^2})^2} \approx 1\,, \tag{A.25}$$

$$F_2 = \frac{1}{(1-\frac{t}{4m^2})(1-\frac{t}{\Lambda^2})^2} \approx 1\,. \tag{A.26}$$

The differential crossection is given by the formula [3]:

$$\frac{16\pi}{\sigma_{tot}^2}\frac{d\sigma}{dt} = \left(\frac{t_c}{t}\right)^2 - 2(\rho+\delta)\frac{t_c}{t} + 1 + \rho^2\,. \tag{A.27}$$

After arithmetics and omitting terms $o(10^{-3}d\sigma/dt))$ - terms with r_5, which was measured to be small in this experiment [2] and terms with $t_c/4m^2$ we have:

$$\frac{A_{NN}+A_{SS}}{2}\frac{d\sigma}{dt} = \frac{\sigma_{tot}^2}{8\pi}\{(\rho-\frac{t_c}{t})\mathrm{Re}\,r_2 + (1-\delta\frac{t_c}{t})\mathrm{Im}\,r_2\}\,, \tag{A.28}$$

$$\frac{A_{NN}-A_{SS}}{2}\frac{d\sigma}{dt} = \frac{\sigma_{tot}^2 t}{16\pi m^2}\{(\rho-\frac{t_c}{t})\mathrm{Re}\,r_4 + (1-\delta\frac{t_c}{t})\mathrm{Im}\,r_4\}\,, \tag{A.29}$$

or

$$\frac{A_{NN}+A_{SS}}{2} = 2\cdot\frac{(\rho-\frac{t_c}{t})\mathrm{Re}\,r_2 + (1-\delta\frac{t_c}{t})\mathrm{Im}\,r_2}{\left(\frac{t_c}{t}\right)^2 - 2(\rho+\delta)\frac{t_c}{t} + 1 + \rho^2}\,, \tag{A.30}$$

$$\frac{A_{NN}-A_{SS}}{2} = \frac{t}{m^2}\cdot\frac{(\rho-\frac{t_c}{t})\mathrm{Re}\,r_4 + (1-\delta\frac{t_c}{t})\mathrm{Im}\,r_4}{\left(\frac{t_c}{t}\right)^2 - 2(\rho+\delta)\frac{t_c}{t} + 1 + \rho^2}\,. \tag{A.31}$$

B Confidence ellipses

When a vector function F_i has several error sources the error by each source is presented by a covariance matrix. Sum of these matrixes produces the total error in case if the sources are independent. An error in a single parameter P gives covariance matrix M_{ij} of elements:

$$M_{ij} = \frac{\partial F_i}{\partial P}\frac{\partial F_j}{\partial P}\sigma_P^2 \approx \Delta_{Fi}\Delta_{Fj}\,, \tag{B.32}$$

where σ_P is the parameter P error and Δ_{Fk} is the deviation of the k-th component of vector F when the parameter P is disturbed by a value of one error: $\Delta_{Fk} = F_k(P+\sigma_P) - F_k(P)$.

For 2-dimential case lines of an equal confidence level are ellipses with half axises A and B, rotated by angle γ. The ellipse parameters sutisfy these equations:

$$tg(2\gamma) = \frac{2M_{01}}{M_{00}-M_{11}}\,, \tag{B.33}$$

$$A^2 + B^2 = M_{00} + M_{11}\,, \tag{B.34}$$

$$A^2 - B^2 = \frac{M_{00}-M_{11}}{cos2\gamma}\,. \tag{B.35}$$

References

[1] N. H. Buttimore, E. Gotsman and E. Leader, Phys. Rev. D **18**, 694 (1978).
T. L. Trueman, hep-ph/0604153.

[2] L. Adamczyk *et al.* [STAR Collaboration], Phys. Lett. B **719**, 62 (2013) [arXiv:1206.1928 [nucl-ex]].

[3] N. H. Buttimore, B. Z. Kopeliovich, E. Leader, J. Soffer and T. L. Trueman, Phys. Rev. D **59**, 114010 (1999) [hep-ph/9901339].

[4] O.V. Selyugin, private communication.

[5] N.H. Buttimore, private communication.

[6] Kin Yip, *Analysis Note for the Single Transverse-Spin Asymmetries (A_N) in elastic p+p collisions at $\sqrt{s} = 200$ GeV*, STAR note PSN0559

[7] R. Battiston *et al.* Nucl. Instrum. Meth. A **238**, 35 (1985).

[8] I. Alekseev et al, *Relative luminosity at pp2pp run 2009*, STAR note PSN0576

[9] https://wiki.bnl.gov/rhicspin/Results

[10] M.L. Goldberger, M.T. Grisaru, S.W. MacDowell and D.Y. Wong, it Phys. Rev. **120** (1960) 2250

[11] R. N. Cahn, *Z. Phys.* **C15** (1982) 253